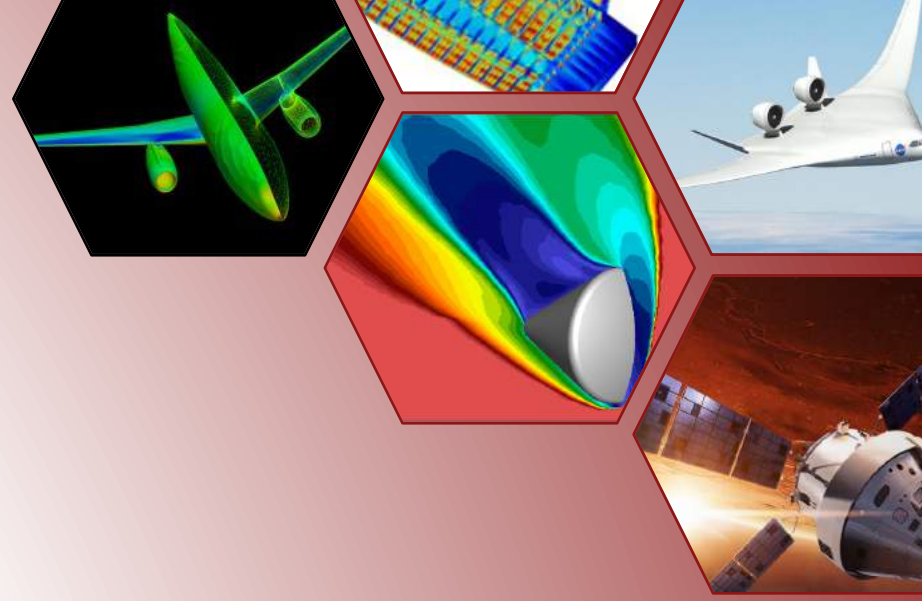
Advanced Modeling and Simulation (AMS) Seminar Series
NASA Ames Research Center, March 10th, 2022



Increasing Modeling Fidelity in the Assessment of Electric Aircraft for Regional and Urban Air Mobility

BY MATTHEW CLARKE

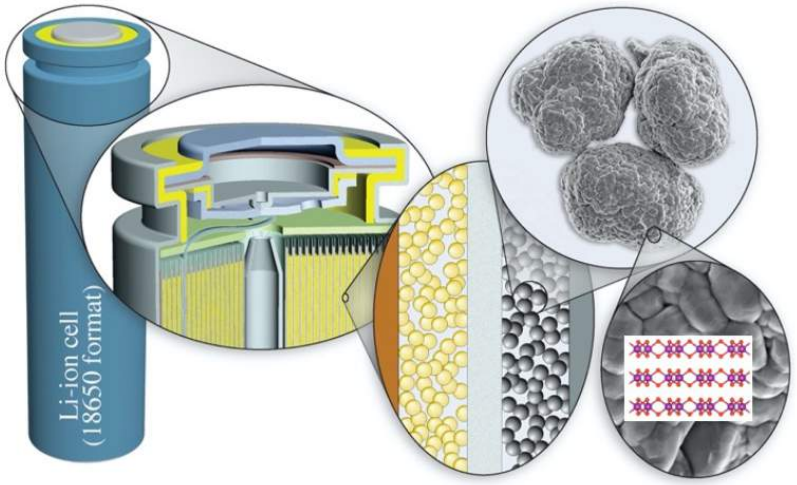
Ph.D. Candidate, Department of Aeronautics and Astronautics

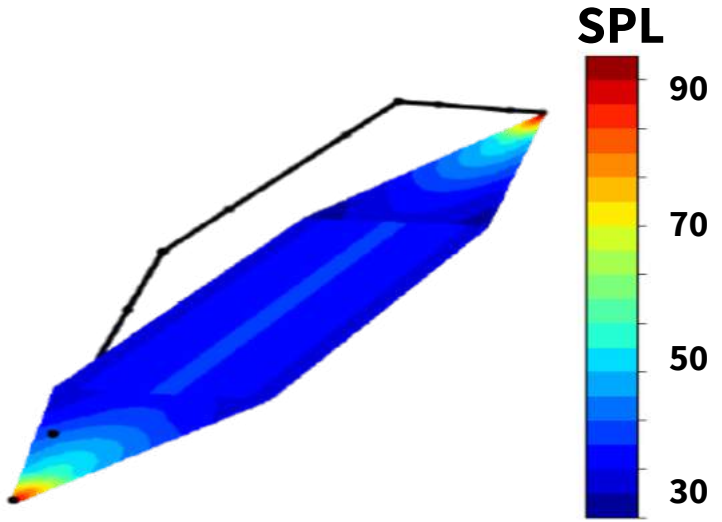
Stanford University

aerospacedesignlab

Terminology and Key Concepts

- **RUAM** – Regional and Urban Air Mobility
- **EC/VTOL** – Electric Conventional/Vertical Takeoff and Landing
- **TAPOOL –** Time-dependent Aircraft Performance Over Operational Lifetime
- **SPL** – Sound Pressure Level
- **Medium-Fidelity Analysis**
  - Captures important physical phenomena.
  - Allows accurate assessment of rotor planform and battery internal structure.



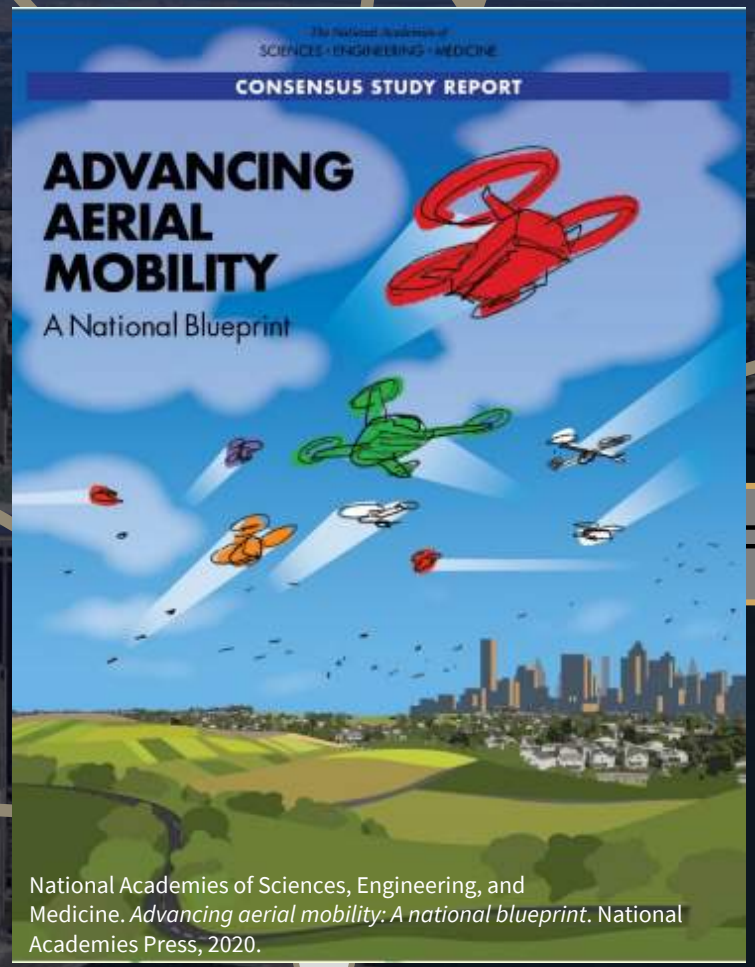


RUAM Application

- Last-mile delivery of packages from local distribution hubs.
- Air-shuttles resembling other transit options such as buses and subways, with regularly scheduled, predetermined routes.
- Ridesharing air-taxis allowing commuters to request pick-up and drop-off destinations.

- Booz Allen Hamilton

LGA



National Academies of Sciences, Engineering, and Medicine. *Advancing aerial mobility: A national blueprint*. National Academies Press, 2020.

FK

EWR

Shortcomings in RUAM Aircraft Design



Accurate estimation of electrochemical cell performance

Fast prediction of RUAM aircraft noise

Research Questions

1. During the aircraft conceptual design phase of non-conventional aircraft, what design-critical nuances can be unearthed through the assessment aircraft performance using medium-fidelity computational methods?
2. What impact does repeated cycling of battery pack over time has on the performance of an electric aircraft?
3. What new performance metrics must be devised to convey findings to a broader audience (market models, flight operation modelers, consumers)?
4. What regions of the flight profile can frequency domain methods provide acceptable estimates of the acoustic footprint of EVTOL aircraft?
5. Can the associations between electric propulsion and aircraft noise be quantified?

Agenda

- PART I: Electric Architecture Modeling
  - Electrification within the Aerospace Industry
  - Lithium-Ion Battery Modeling for Aerospace Applications[1]
  - Estimating the Operational Lifetime of Battery Powered Aircraft[2]
- PART 2: Rotorcraft Noise
  - Medium-Fidelity Noise Prediction
  - Rotor Blade Design Optimization[3]
  - Comparison of Vehicle Acoustic Footprint
- PART 3: System Analysis of EC/VTOL aircraft

1. Clarke, Matthew, and Juan J. Alonso. "Lithium–Ion Battery Modeling for Aerospace Applications." *Journal of Aircraft* 58.6 (2021): 1323-1335
2. Clarke, Matthew, and Juan J. Alonso. “Forecasting the Operational Lifetime of Battery-Powered Electric Aircraft Using TAPOOL Diagrams “*Journal of Aircraft* (under review)
3. Clarke, Matthew, and Juan J. Alonso. “Accelerated Rotor Blade Optimization for RUAM Applications“ *AIAA Journal (manuscript in preparation)*

Electrification within the Aerospace Industry

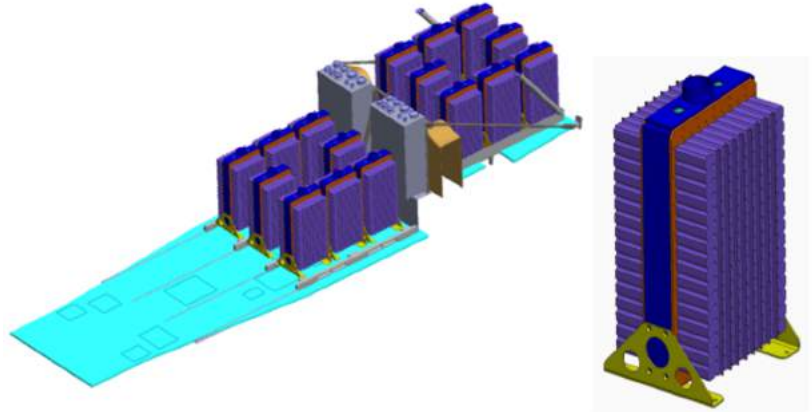
Internal Combustion Engine (ICE) vs. Distributed Electric Propulsion (DEP) Architectures, NASA (2019)

	ICE	DEP
Average Operating cost per hour	$ 440	$ 275
% Operating Cost per hour	45 %	9 %
Greenhouse Gases emission	90 kg (CO_2)/hr.	10 - 24 kg (CO_2)/hr.

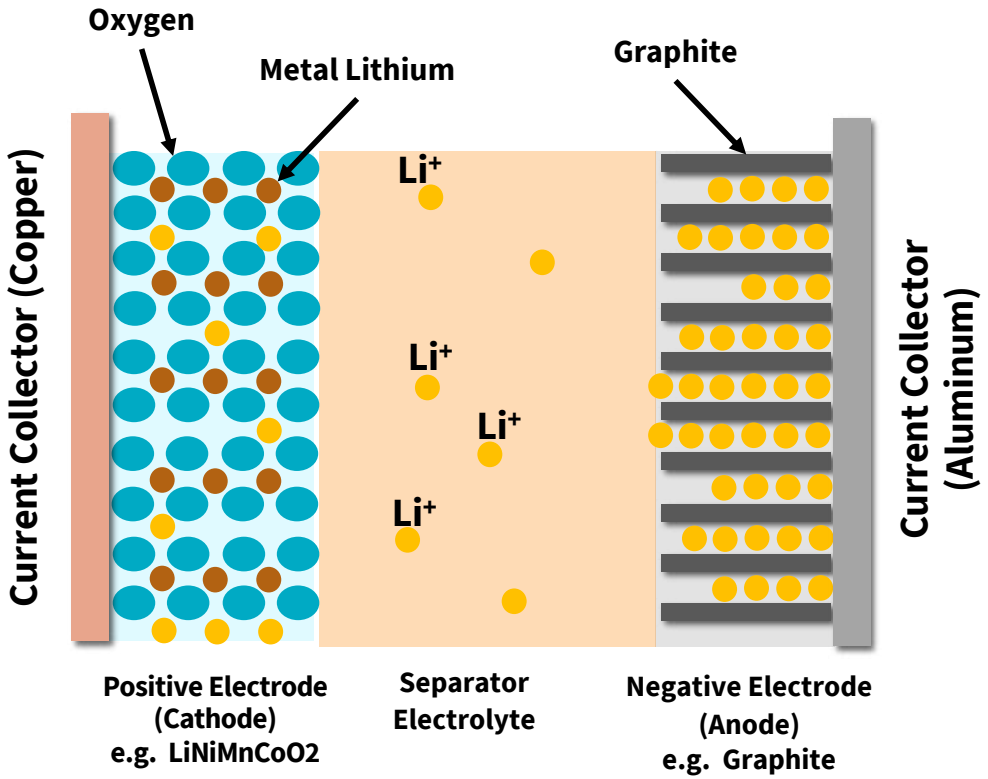
NASA X-57 Maxwell

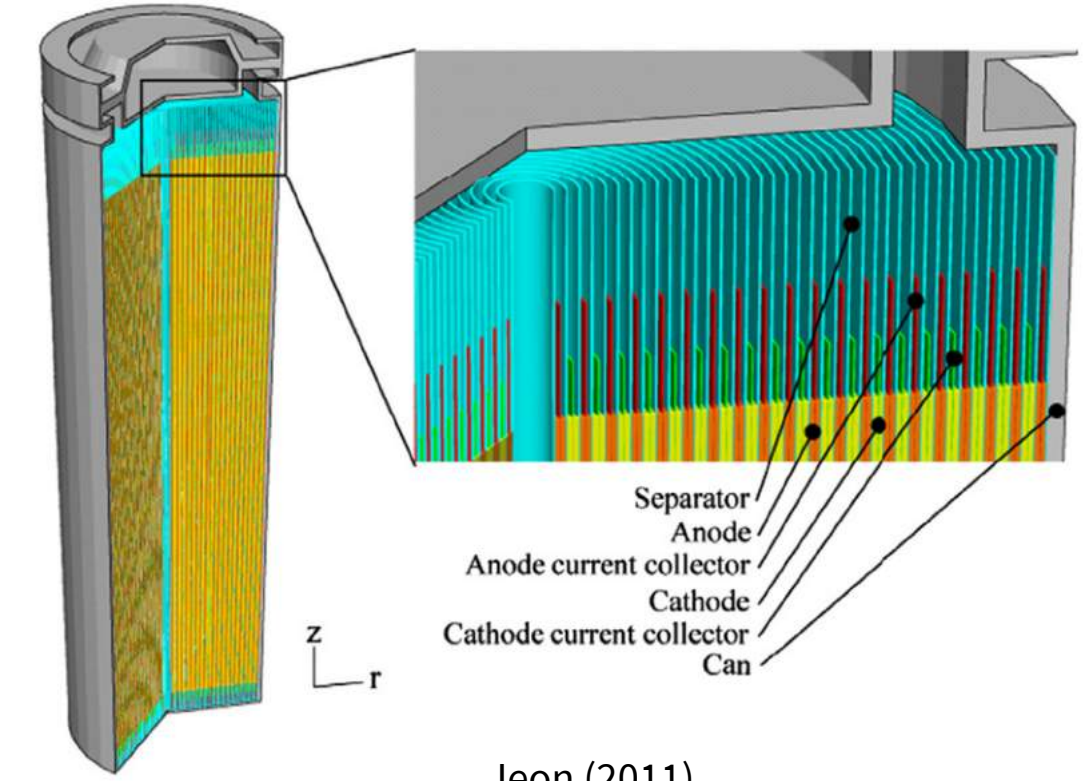


X57 Battery Module Network, Chin, (2018)



Anatomy of the Lithium-Ion Battery



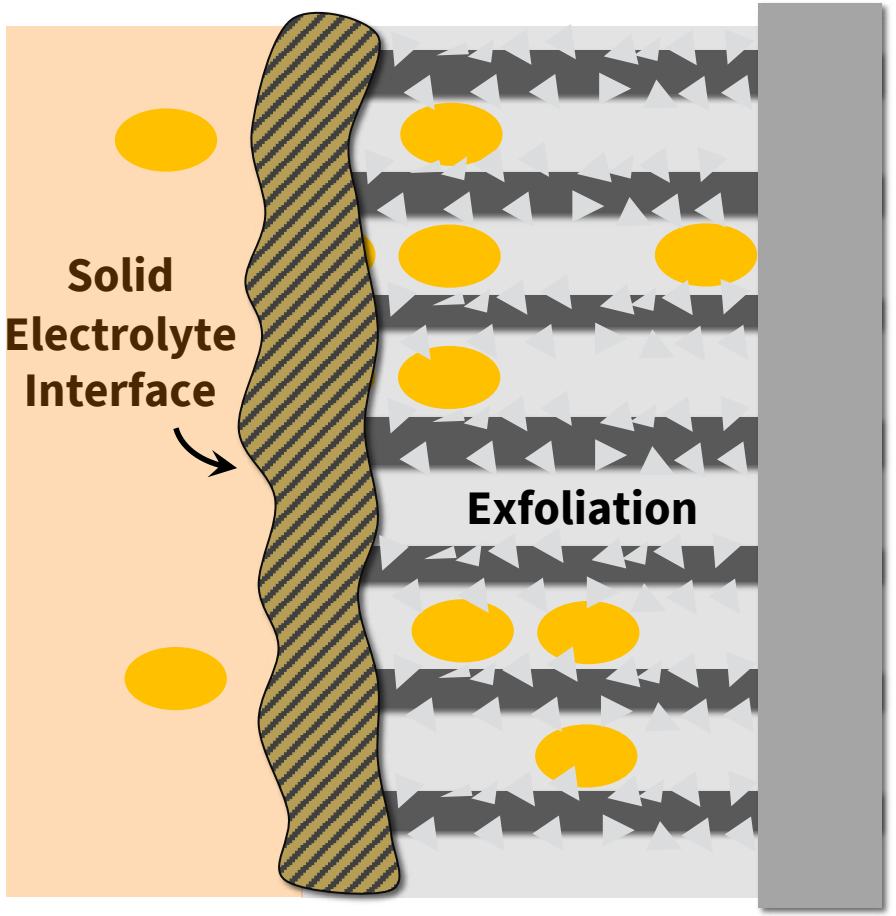


Jeon (2011)

Addressing Shortcomings of Battery Modeling in Conceptual Design

Little emphasis has been placed on quantifying battery state of health

- Stress factors enhance physical-chemical mechanisms within the cell
- Performance degrades as a result of:
  - Repeated cycling
  - Thermal stresses due to internal resistance heat dissipation
  - The growth of a Solid Electrolyte Interphase (SEI) film around the cathode
  - Exfoliation of the oxidized layers reduces the ability of ions to electronically bind to the anode



Key Objectives

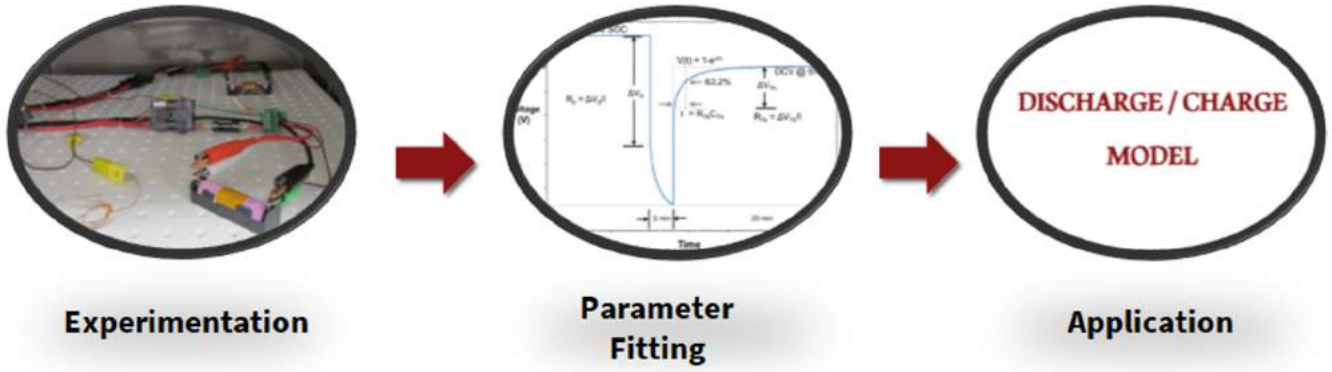
Outline — Outline the implementation of a discharge and aging model for a lithium-ion batteries

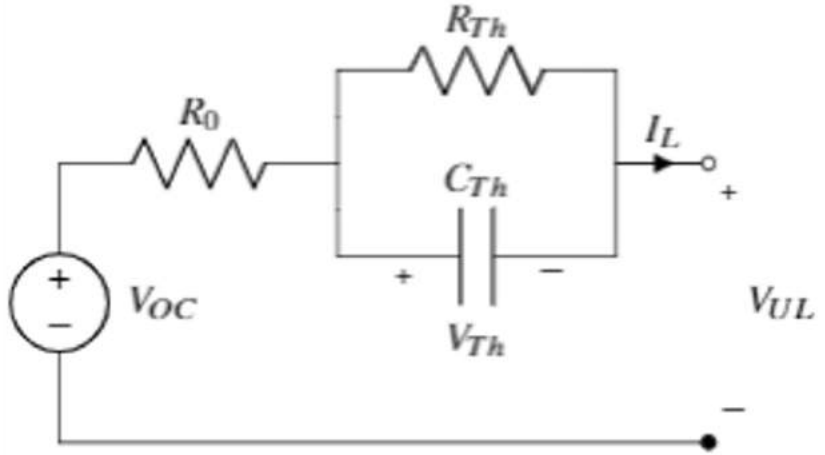
Predict — Predict the cycle-life of an electric aircraft provided with the flight profile using experimentally obtained parameters for characterizing aging.

Identify — Identify the sensitivity of battery chemistry, rates of climb and descent, and range on discharge rate, cycle-life and state of health.

Approach: Electrical Discharge Model

- Semi-empirical model based on the Thevenin circuit
- Capable of characterizing key properties of discharge such as the transient state.
- Adaptable for different cell chemistries.
- Fitting parameters (V_{OC} , R_0 , V_{Th} , R_{Th} , τ_{Th}) obtained through experimental tests.





Thevenin Equivalent Circuit Discharge/Charge Model

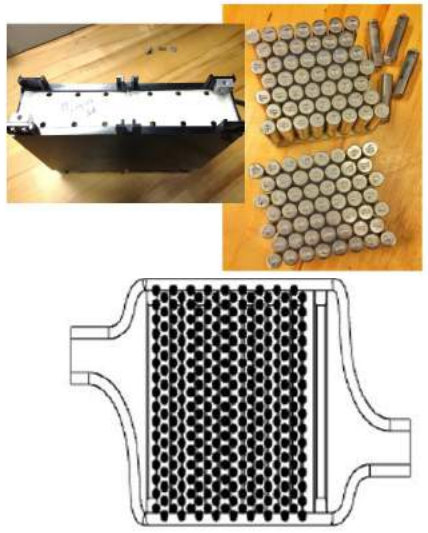
$$C_{Th} = \frac{\tau_{Th}}{R_{Th}}$$

$$\frac{dV_{Th}}{dt} = \frac{I_L}{C_{Th}} - \frac{V_{Th}}{R_{Th}C_{Th}}$$

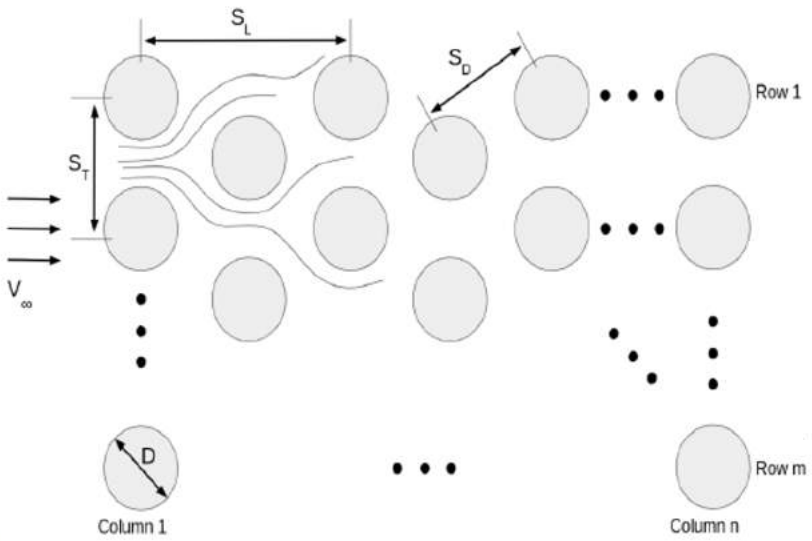
$$V_{UL} = V_{OC} - V_{Th} - I_L R_0$$

Approach: Thermal Model

- Temperature and heat-generation within each cell is determined through conservation of energy and Gibbs function using a relation proposed by Bernardi (1984)
- Thermodynamic changes are captured through numerical expressions for the electrochemical reactions, phase changes, mixing effects and Joule heating



(a) Representative battery module with $N_L = 30, N_T = 16$.



(b) Staggered cell arrangement.

Heat Generation

$$\dot{q}_{heat} = \dot{q}_{Joule} + \dot{q}_{entropy}$$

$$\dot{q}_{Joule} = A_e i(V_{OC} - V_{UL}) = \frac{i^2}{\sigma}$$

$$\dot{q}_{entropy} = -I\left(T\frac{\delta V_{OC}}{\delta T}\right) = -T\Delta S\frac{i}{nF}$$

Heat Removal

$$\dot{q}_{convec} = N_{tot}\tilde{h}A_s\Delta T_{LM}$$

Approach: Thermal Model

- The average heat transfer coefficient for the entire module can be determined using the relationship between Nu and Re.

$$\tilde{h} = \frac{Nu \cdot k_f}{D} \qquad \text{where } Nu = CRe_{D,max}^{m} Pr^{0.36} \left(\frac{Pr}{Pr_w}\right)^{0.25}$$

$$\begin{cases} C = 0.35\left(\frac{S_T}{S_L}\right)^{0.2} \text{ and } m = 0.6, & \text{if } Re_{D,max} > 1\text{x}\,10^3 \\ C = 0.51 \text{ and } m = 0.5, & \text{otherwise} \end{cases}$$

- The temperature difference between the cell surface and the outlet temperature can then be determined:

$$\frac{T_w - T_o}{T_w - T_i} = \frac{exp(-\pi D N_{tot} h)}{(\rho_\infty V_\infty N_T S_T c_{p_\infty})}$$

$$\Delta T_{LM} = \frac{(T_w - T_i) - (T_w - T_o)}{log\left(\frac{T_w - T_i}{T_w - T_o}\right)}$$

T_w = cell surface (wall) temperature
T_i = inlet temperature
T_o = outlet temperature
N_{tot} = total number of cells in module

Approach: Cell Degradation (Aging) Model

- Based on a model developed by Schmalstieg (2014) that fits a physics-based model to experimental parameters to characterize aging.
- Calendar Aging

$$\alpha_{cap}(T,V) = (7.543 \cdot V - 23.75) \cdot 10^6 \cdot e^{\frac{-6976}{T}}$$

$$\alpha_{res}(T,V) = (5.270 \cdot V - 16.32) \cdot 10^5 \cdot e^{\frac{-5976}{T}}$$

- Cycle Aging

$$\beta_{cap} = 7.348 \cdot 10^{-3} \cdot (\emptyset V - 3.667)^2 + 7.600 \cdot 10^{-4} + 4.081 \cdot 10^{-3} \cdot \Delta DOD$$

$$\beta_{res} = 2.153 \cdot 10^{-4} \cdot (\emptyset V - 3.725)^2 - 1.521 \cdot 10^{-5} + 2.798 \cdot 10^{-4} \cdot \Delta DOD$$

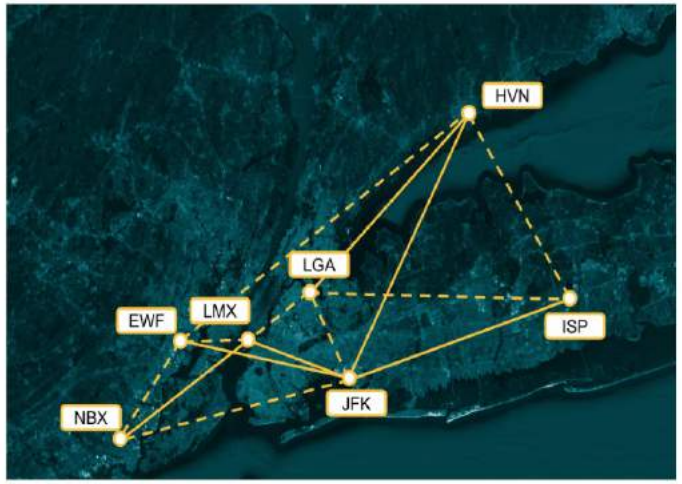
- Capacity Fade Model

$$E_{fade} = 1 - \alpha_{cap} \cdot t^{0.75} - \beta_{cap} \cdot \sqrt{Q}$$

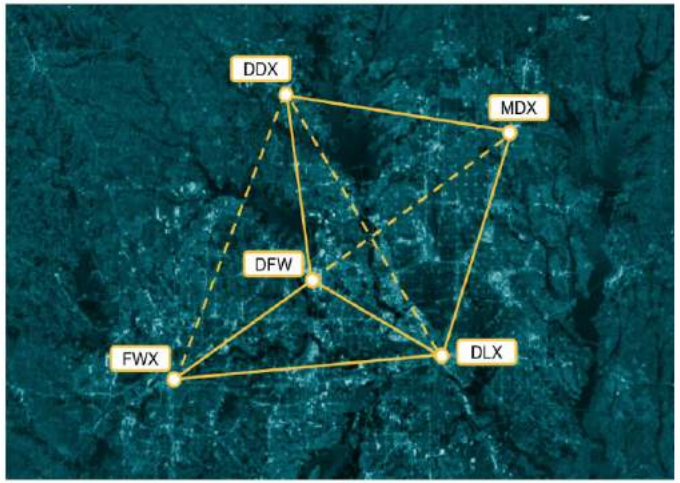
- Internal Resistance Growth Model

$$R_{growth} = 1 + \alpha_{res} \cdot t^{0.75} + \beta_{res} \cdot Q$$

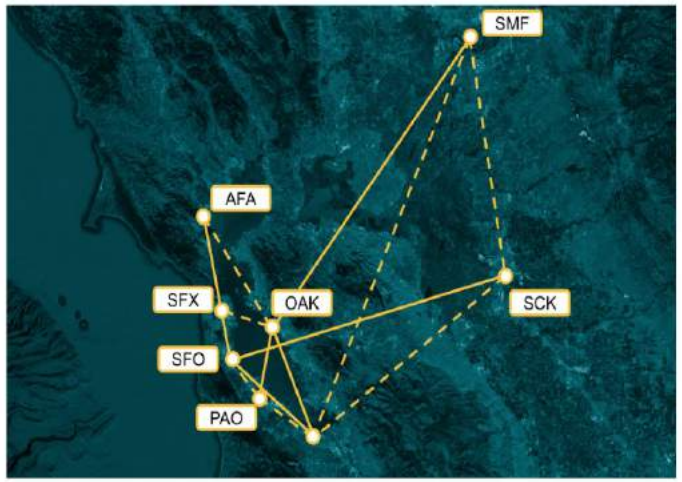
RUAM Potential Business Cases



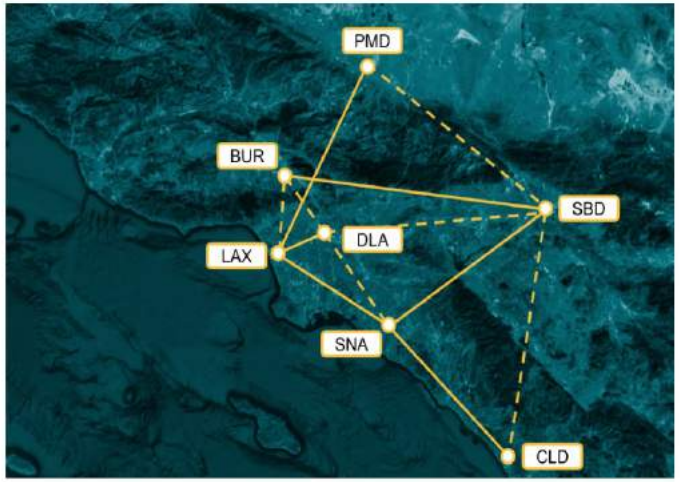
(a) New York Metropolitan Area, NY.



(b) Dallas-Fort Worth Metropolitan Area, TX.



(c) San Francisco Bay Metropolitan Area, CA.

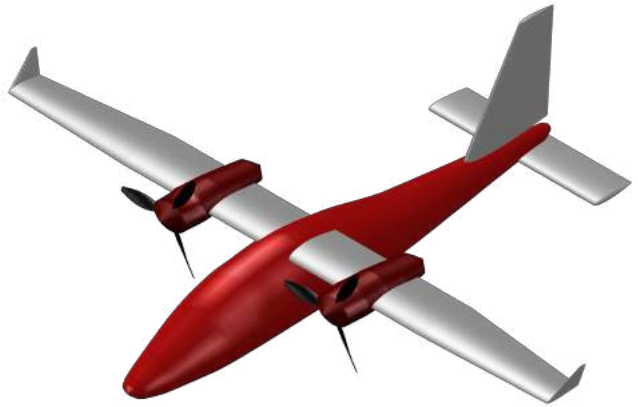


(d) Los Angeles Metropolitan Area, CA.

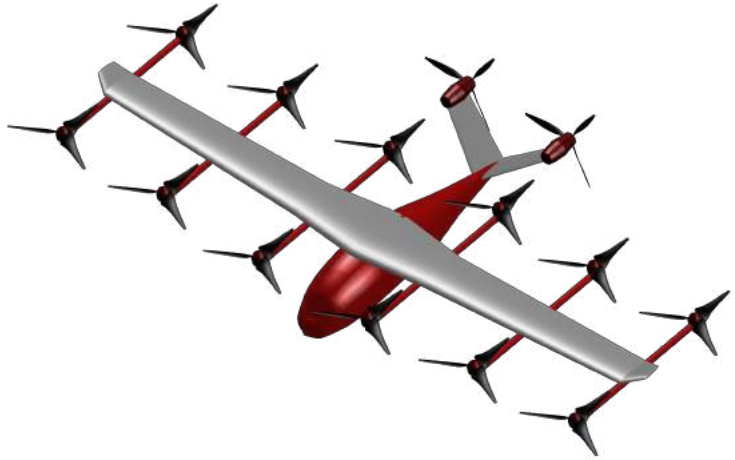
Metropolitan Area	Route	Range (nmi)
San Francisco Bay Metropolitan Area	SFO - SJC	26
	OAK - SMF	78
	OAK - SJC	26
	PAO - OAK	17
	AFA - SFO	21
	SFO - SCK	56
New York Metropolitan Area	LMX* - JFK	10
	HVN - LGA	55
	EWF - JFK	21
	NBX* - LMX*	26
	HVN - JFK	50
	JFK - ISP	50
Los Angeles Metropolitan Area	LAX - SNA	31
	SBD - SNA	41
	BUR - SBD	53
	DLA* - LAX	10
	SNA - CLD	35
	PMD - LAX	44
Dallas - Fort Worth Metropolitan Area	DLX - DFW	27
	DFW - DLX*	13
	DFW - FWX*	16
	MLX* - DLX*	28
	FWX* - DDX*	37
	MLX* - DDX*	25

Common Reference Models

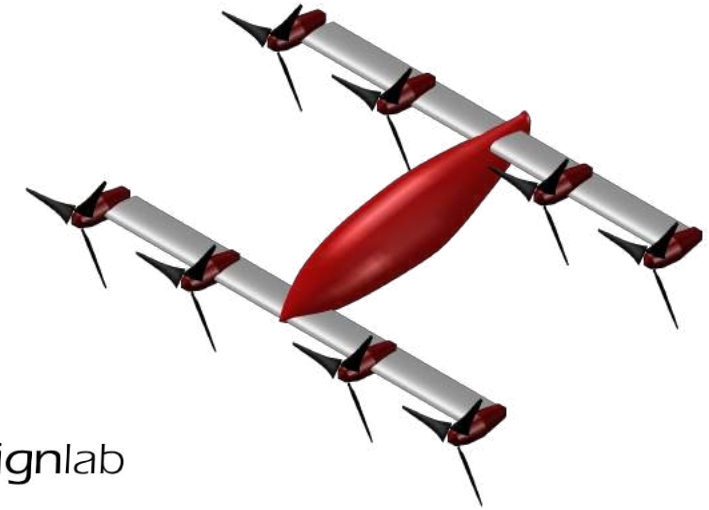
Twin-engine ECTOL



Stopped-Rotor EVTOL



Tandem Tiltwing EVTOL



Hexacopter EVTOL

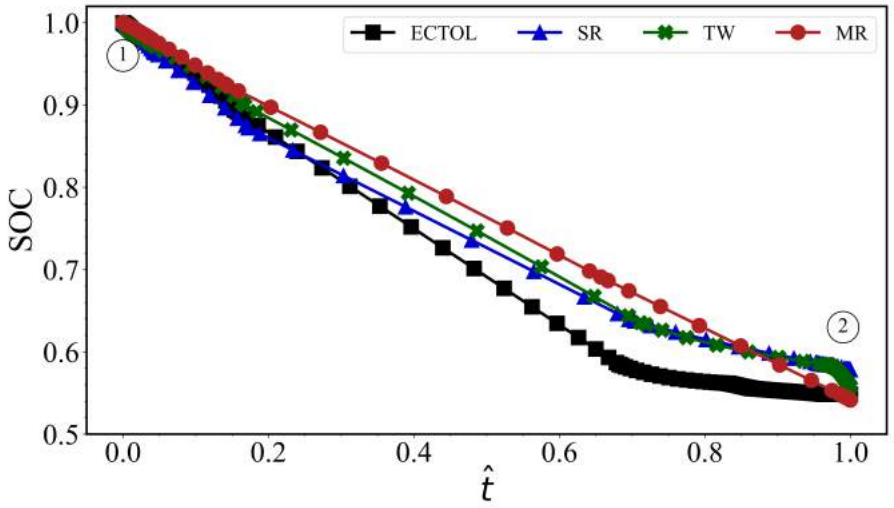


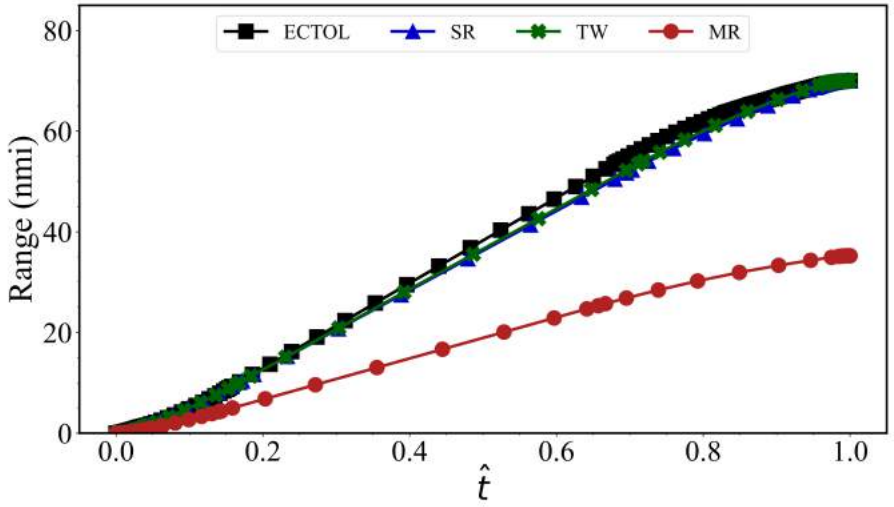
Flight Operation Simulations

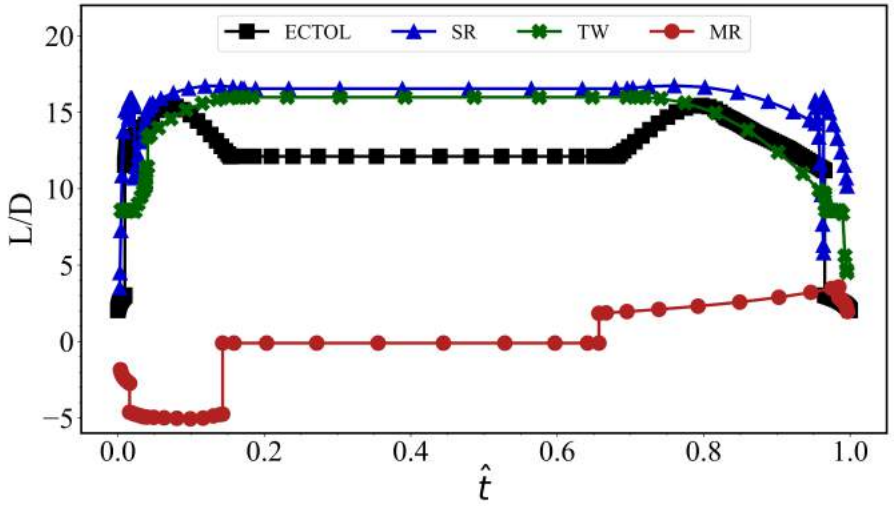
- One year of operation
- Eight daily flights - reflects continuous services that UAM businesses are expected to operate.
- Recharging at 1C from the end-of-flight is simulated after each flight

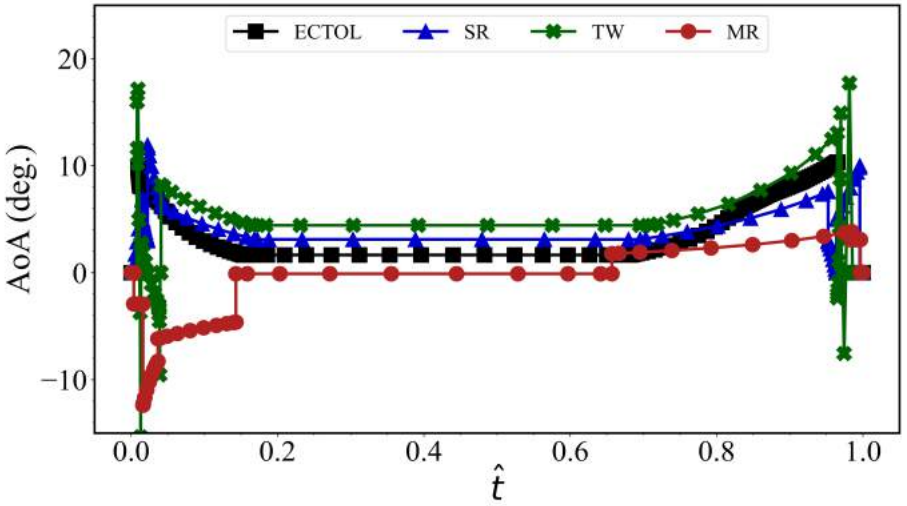
Segment	Twin-engine ECTOL	Stopped-rotor	Tilt-wing	Hexacopter
1	Take-off	Vertical Climb	Vertical Climb	Vertical Climb
2	Departure End of Runway	Vertical Transition	Vertical Transition	Vertical Transition
3	Initial Climb Area	Climb Transition	Climb Transition 1	Climb
4	Climb	Climb 1	Climb Transition 2	Cruise
5	Cruise	Climb 2	Climb	Descent
6	Descent	Cruise	Cruise	Descent Transition
7	Downleg	Descent	Descent	Vertical Descent
8	Baseleg	Approach Transition	Approach Transition	
9	Final Approach	Descent Transition	Descent Transition	
10	Landing	Vertical Descent	Vertical Descent	
11	Reverse Thrust			

RUAM Aircraft Performance

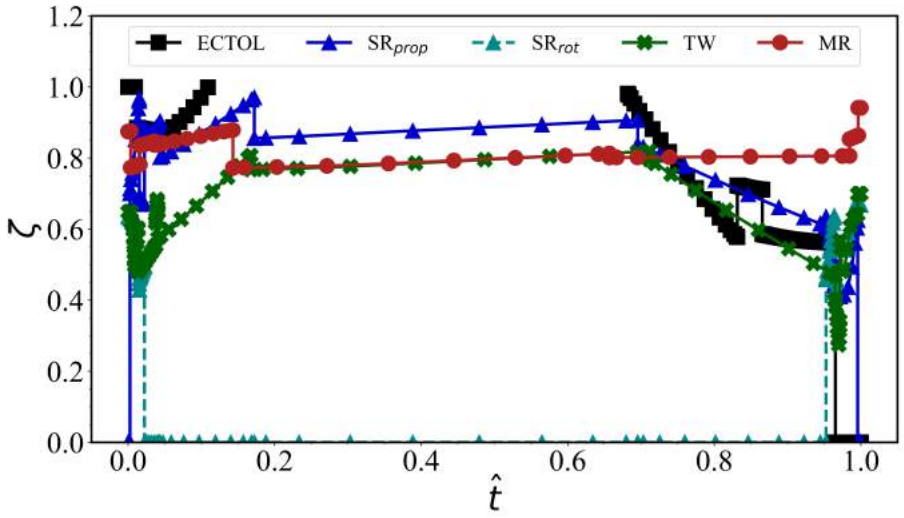


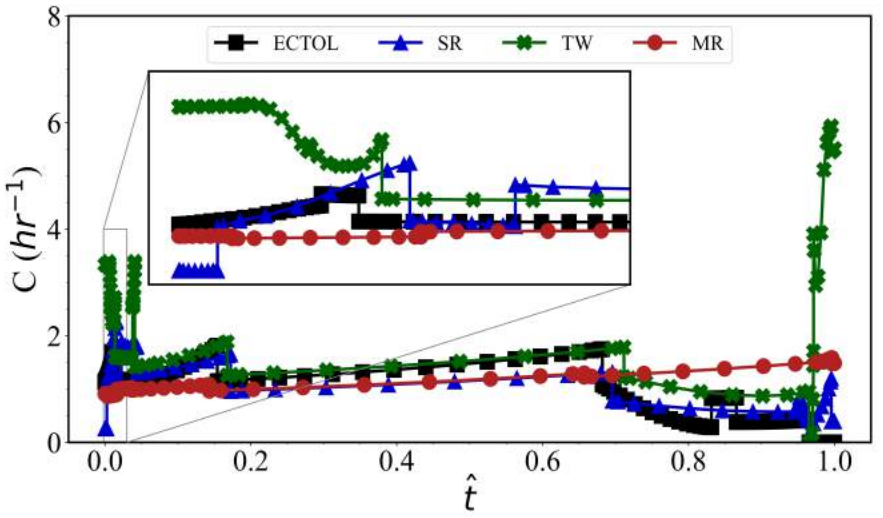


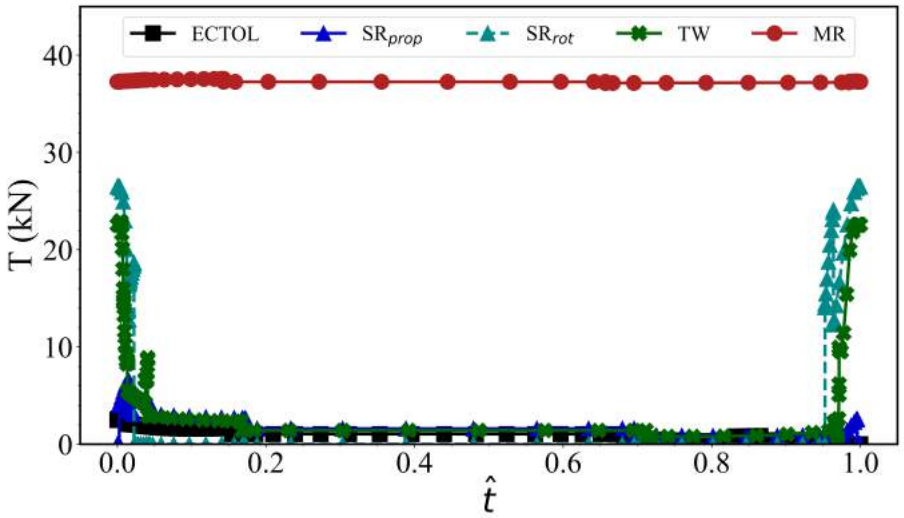


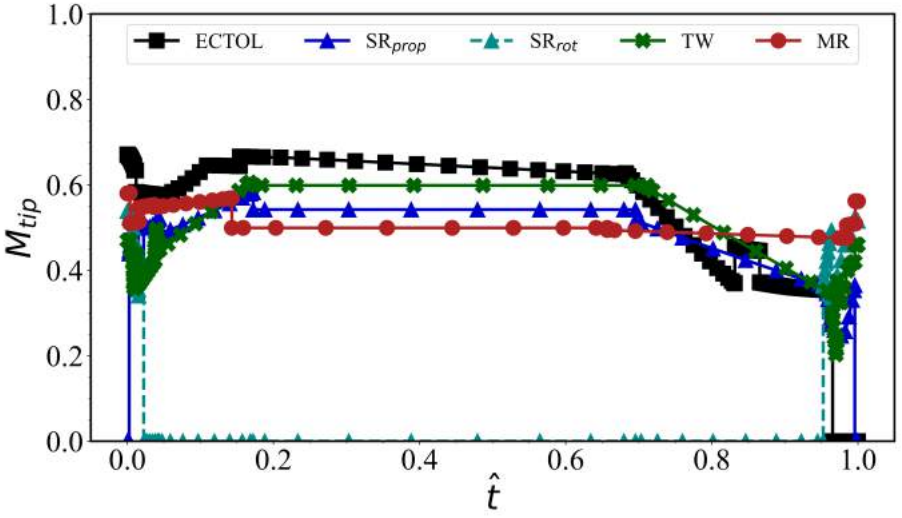


RUAM Aircraft Performance

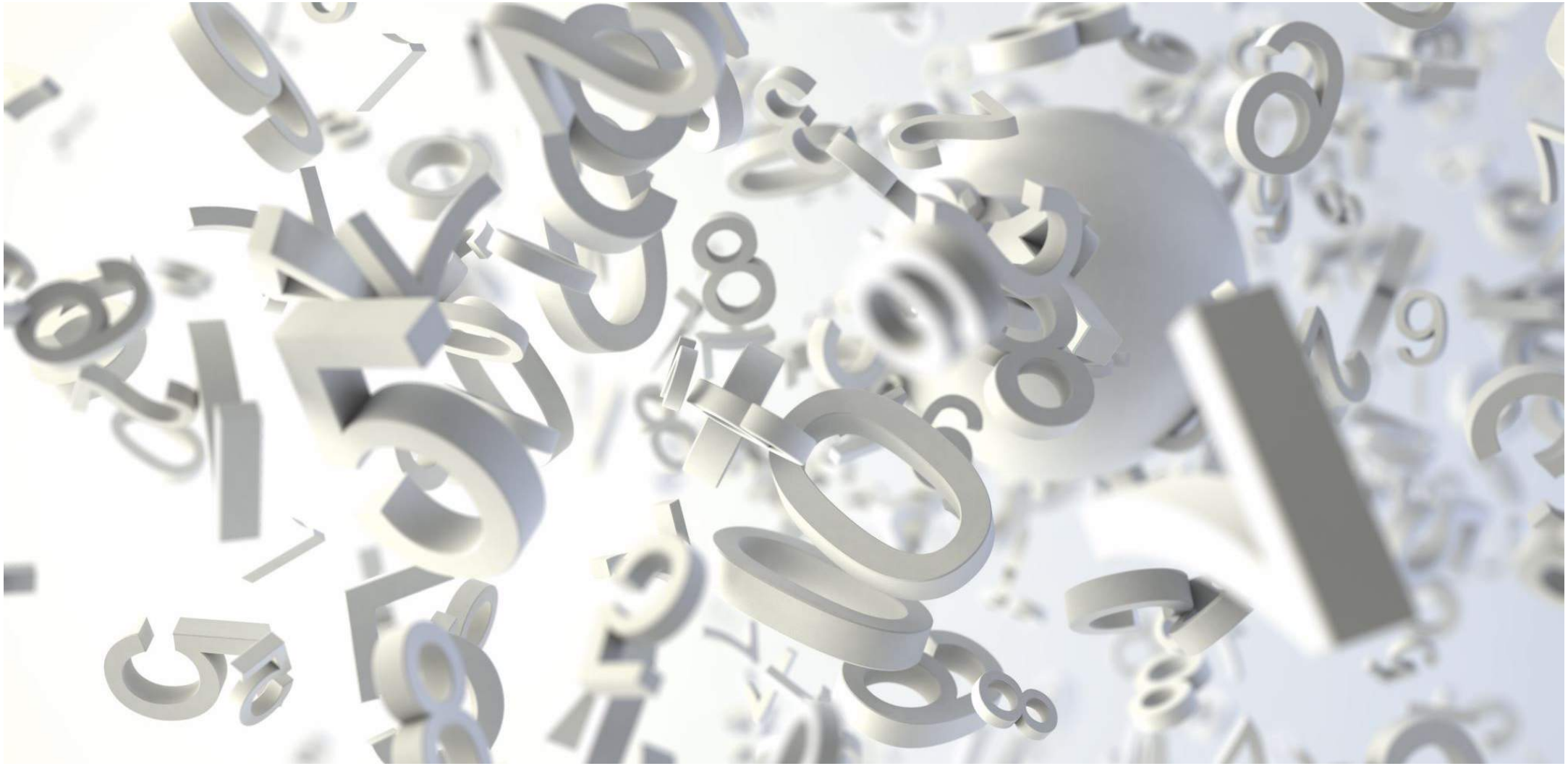








How do we convey large amounts of data?



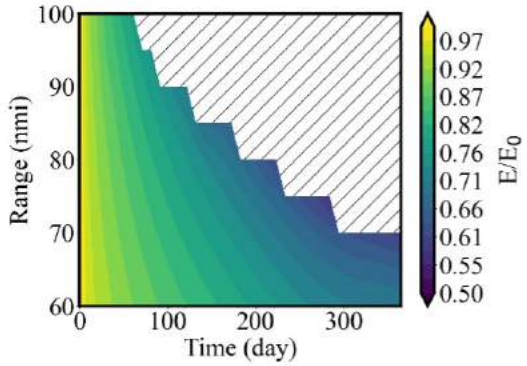
Time-dependent Aircraft Performance Over Operational Lifetime (TAPOOL) Diagrams

Describes the behavior of an electric aircraft's battery pack under realistic flight and environmental conditions.

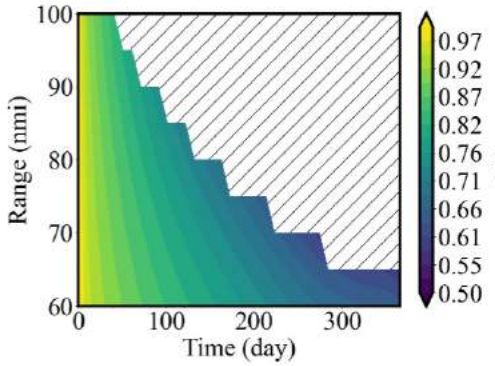
Differs from traditional approaches of assessing battery-powered aircraft in two ways:

Time-dependency is introduced into the efficiency of stored-energy systems	Use of the full flight profile

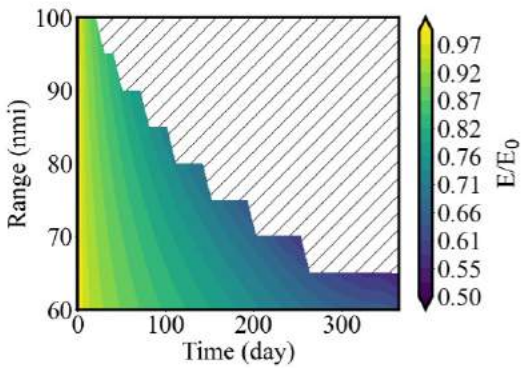
Battery Capacity TAPOOL Diagram



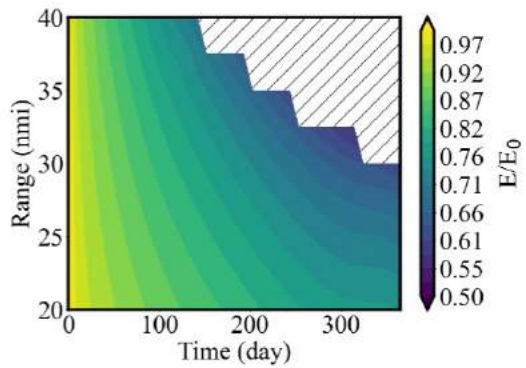
(a) Twin-engine ECTOL aircraft.



(b) Stopped-rotor EVTOL aircraft.



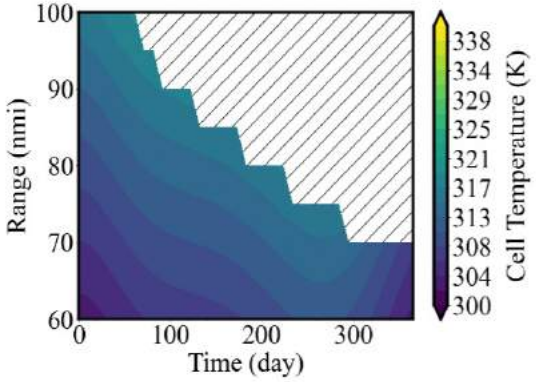
(c) Tiltwing EVTOL aircraft.



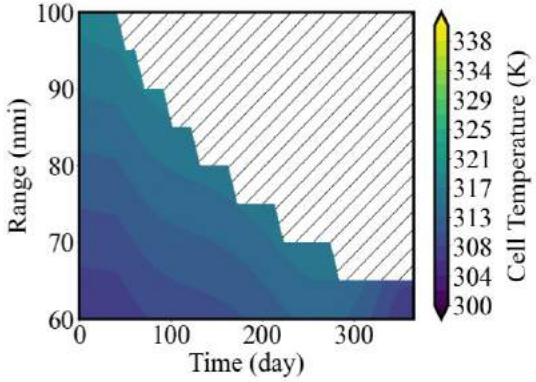
(d) Hexacopter EVTOL aircraft.

- Longer missions accelerate cell degradation and reduce the operational lifetime.
- Operational lifetime of the ECTOL, stopped-rotor, tilt-wing and hexacopter decreases by 11, 8, 9 and 23 days respectively for every additional nautical mile flown.
- The above plots also lend key insights into what strategies air-shuttle and air-taxi services should adopt to maximize the potential of both brand-new and used aircraft.

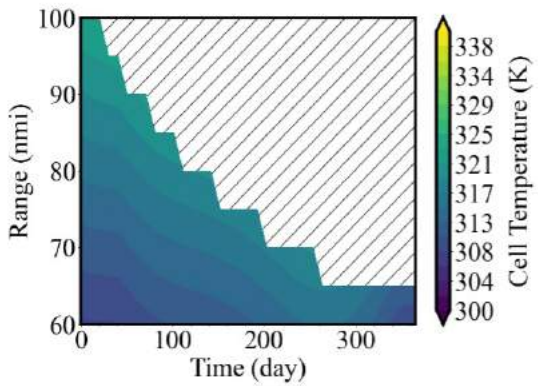
Temperature TAPOOL Diagram



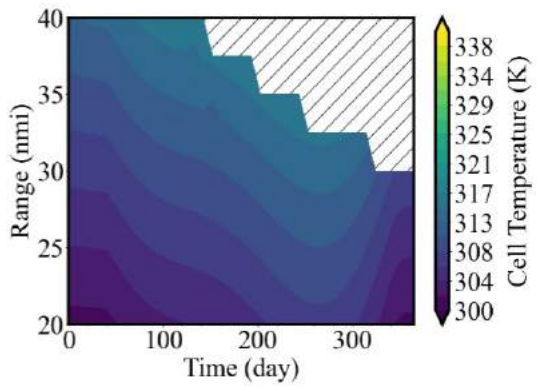
(a) Twin-engine ECTOL aircraft.



(b) Stopped-rotor EVTOL aircraft.



(c) Tiltwing EVTOL aircraft.



(d) Hexacopter EVTOL aircraft.

- Accompanying the increase in ohmic resistance is the increase in cell temperature.
- Exhibits strong bi-variance and is offset by the ambient temperature which changes year-round.
- The temperature TAPOOL diagram provides system designers with critical insights into the design of thermal management system and the cell layout needed to achieve ideal operating conditions.

Future Direction for Battery Modeling Research

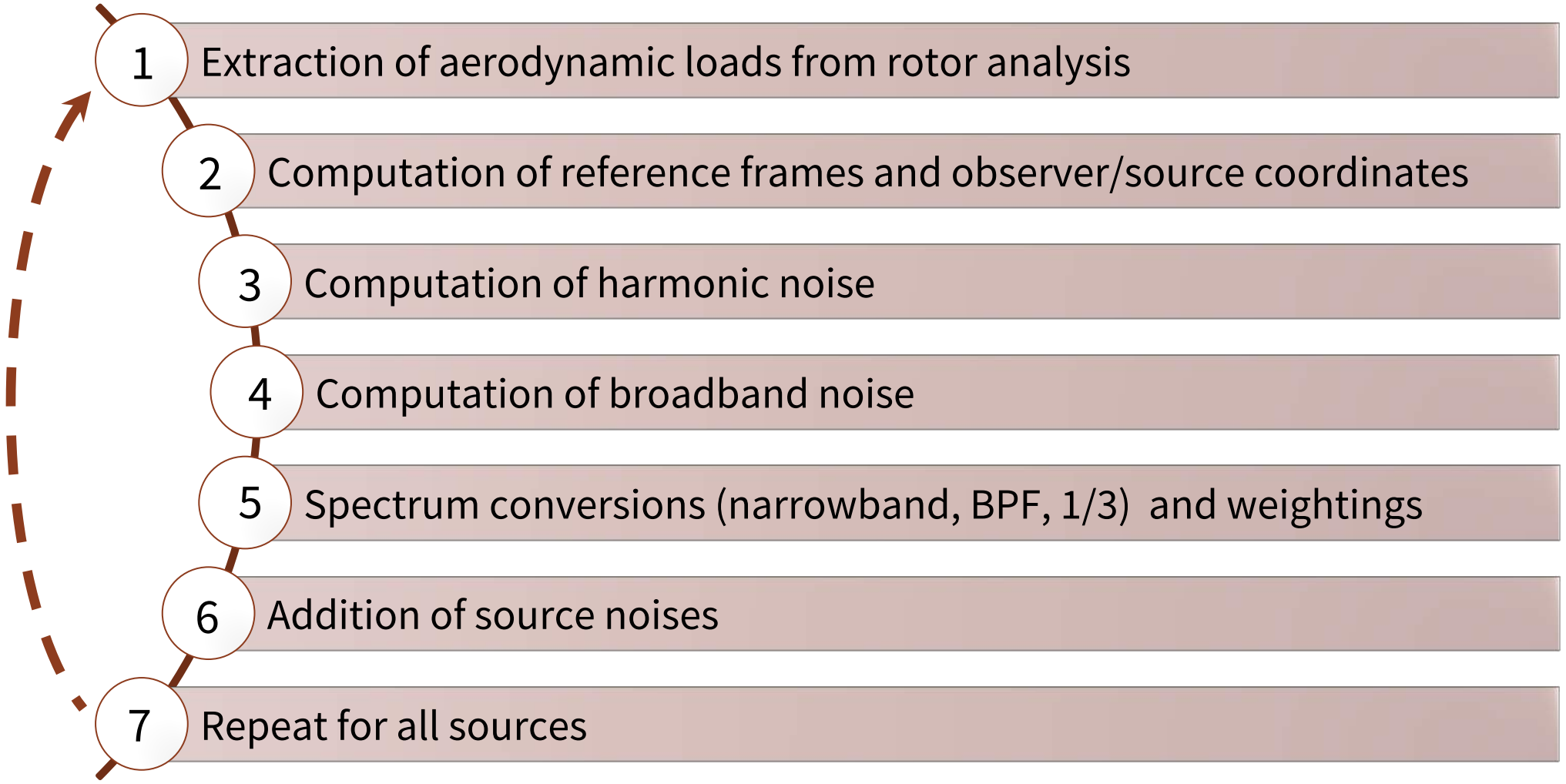
- Improvement of state-variable prediction via electrochemical models
- Experimental testing and documentation of stress factors that enhance physical-chemical mechanisms
- Cell inverse-design
- BMS thermal management algorithm development
- Maximizing aircraft utility through evolving flight operations

Regional and Urban Air Mobility Aircraft Noise

- Community noise exposure is an integral factor in vertiport placement
- Acoustic footprint of EC/VTOL aircraft will dictate approach and departure air-corridors
- Current noise prediction methods fall on the extremities of the computational cost-accuracy spectrum
- There is a need for a tool for iterative conceptual design



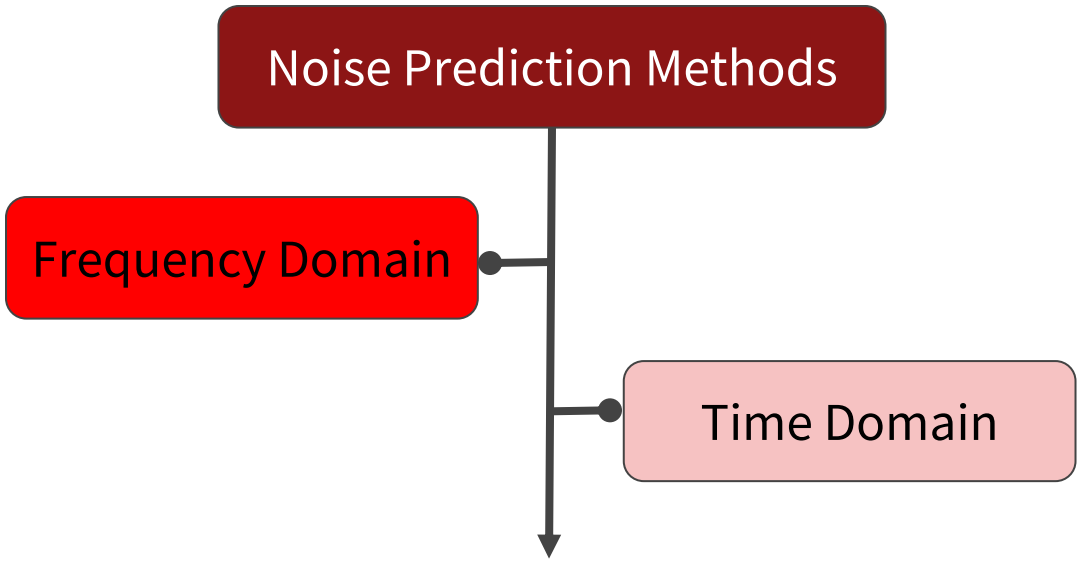
Methodology of SUAVE's Fidelity One Noise Prediction



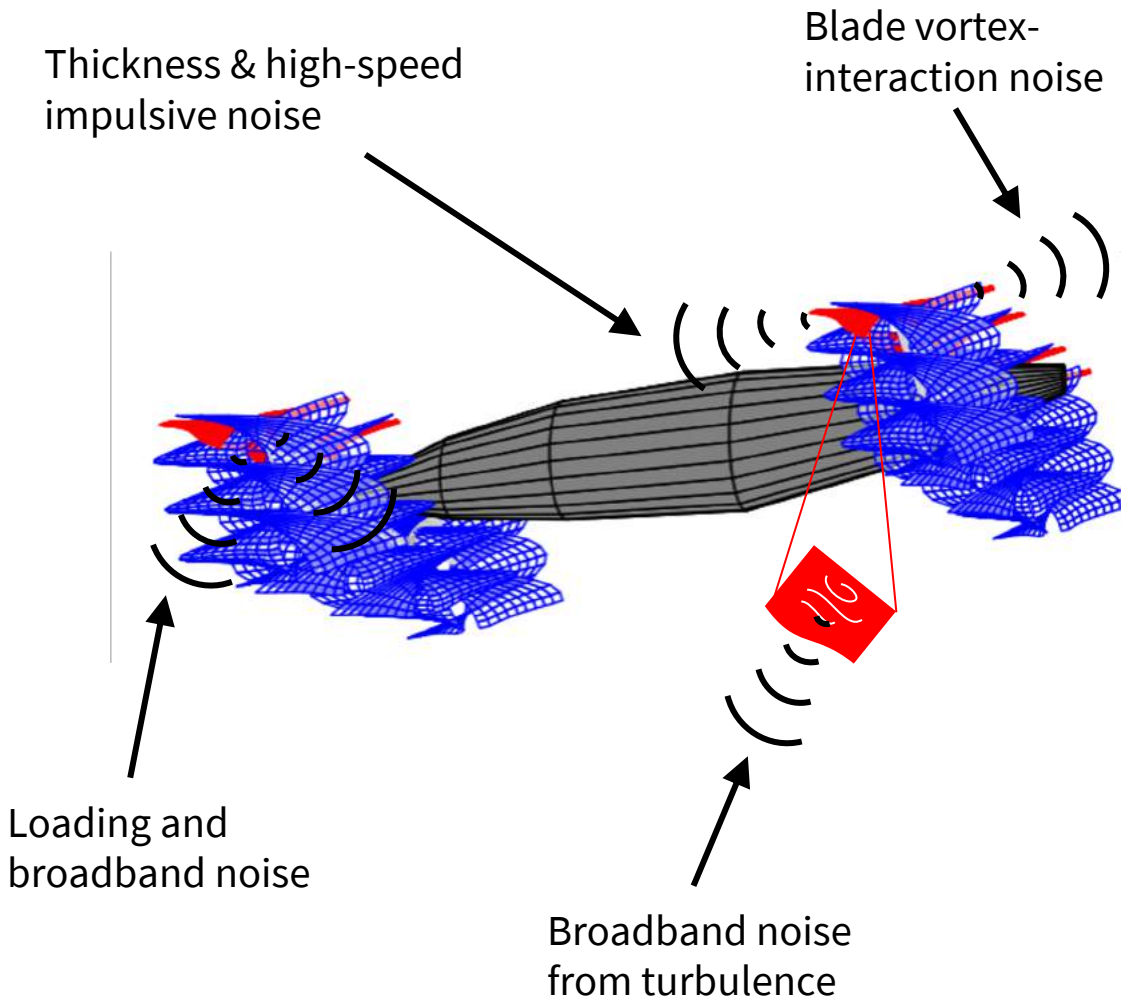
Computational Noise Prediction

- Starting with the governing equation of sound generation: Goldstein's version of the acoustic analogy

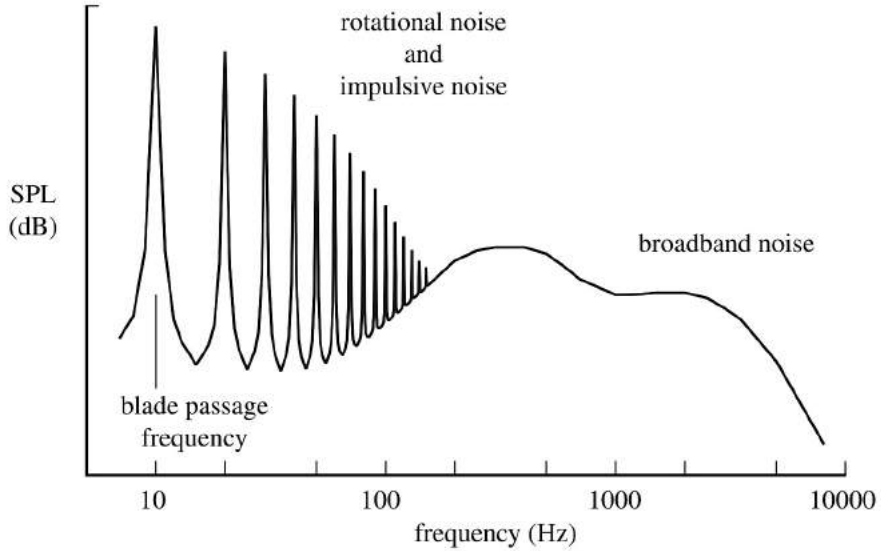
$$\rho'(x,t) = -\frac{1}{c_0^2}\int_{-T}^{T}\int_{S(\tau)}\left(\rho_0 V_n \frac{\partial G}{\partial \tau} + f_i \frac{\partial G}{\partial y_i}\right) \mathrm{d}S(y)\mathrm{d}\tau + \frac{1}{c_0^2}\int_{-T}^{T}\int_{\nu(\tau)} T_{ij}\frac{\partial^2 G}{\partial y_i \partial y_j}\,\mathrm{d}y\,\mathrm{d}\tau$$



Aeroacoustics of Rotorcraft



- Rotational/harmonic noise
  - Thickness noise, P_T
  - Loading noise, P_L
- Broadband noise
  - vortex(self) noise, P_V
- Interaction and distortional effects



Harmonic Noise

- The equations for loading and thickness noise contribution to the total root mean square sound pressure at each harmonic, m are presented below in retarded coordinates.

- Loading

$$P_{m_L} = \frac{imBM_t \sin\theta_r \exp\left[imB\left(\frac{\Omega S_r}{c} + \left(\phi' - \frac{\pi}{2}\right)\right)\right]}{2\sqrt{2}\pi Y r_t \left(1 - M_x \cos\theta_r\right)} \int_{hub}^{tip} \left[\frac{\cos\theta'_r}{1 - M_x \cos\theta_r}\frac{dT}{dr} - \frac{1}{r^2 M_t r_t}\frac{dQ}{dr}\right] \exp\left(i\phi_s\right) J_{mB} \Psi_L dr$$

- Thickness

$$P_{m_T} = \frac{-\rho c^2 B \sin\theta_r \exp\left[imB\left(\frac{\Omega S_r}{c} + \left(\phi' - \frac{\pi}{2}\right)\right)\right]}{4\sqrt{2}\pi (Y/D)\left(1 - M_x \cos\theta_r\right)} \int_{hub}^{tip} M_s^2 (h/b) \exp\left(i\phi_s\right) J_{mB} k_x^2 \Psi_V dr$$

where

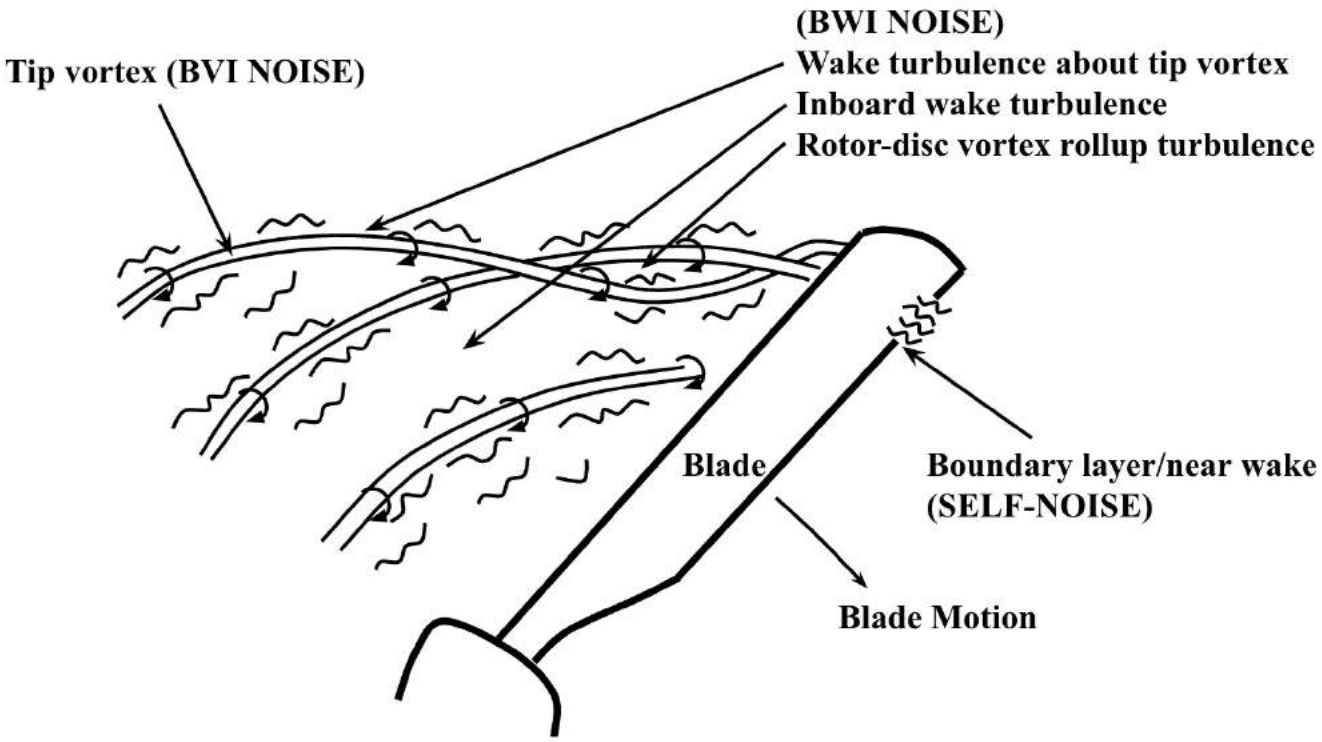
$$k_x = \frac{2mBbM_t}{M_s\left(1 - M_x \cos\theta_r\right)}$$

$$\phi_s = \frac{2mBM_t}{M_s\left(1 - M_x \cos\theta_r\right)}\frac{MCA}{D}$$

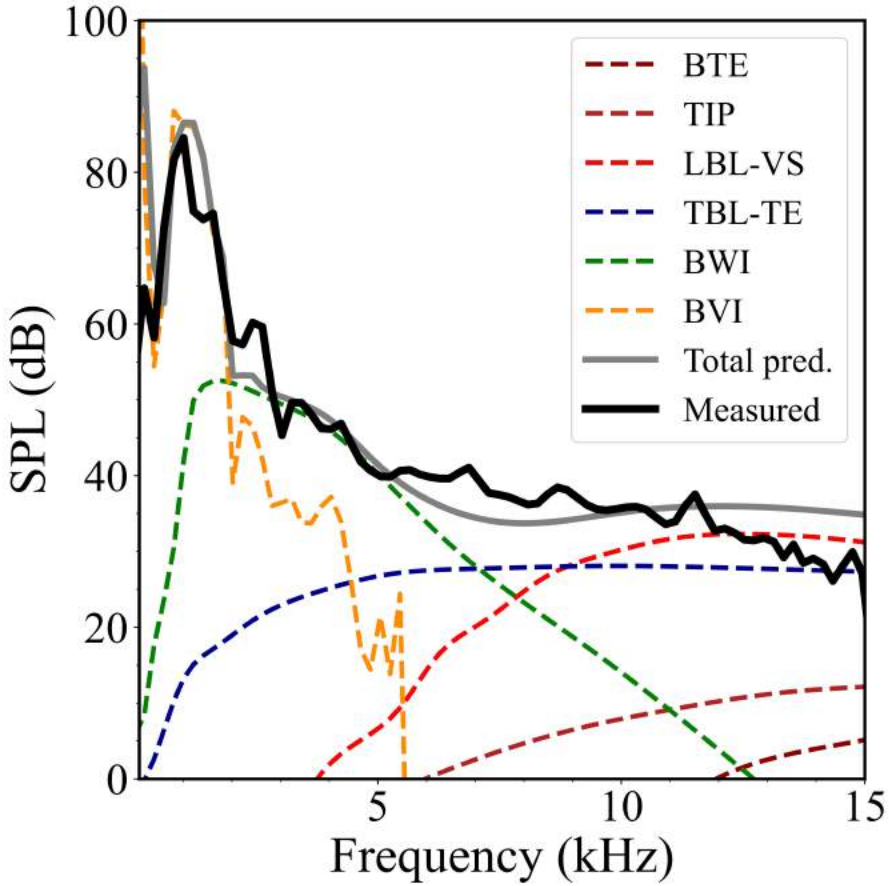
$$J_{mB} = J_{mB}\left(\frac{mBrM_t \sin\theta'_r}{1 - M_x \cos\theta_r}\right)$$

Source: Hanson (1995)

Broadband Noise



Brooks (2001)

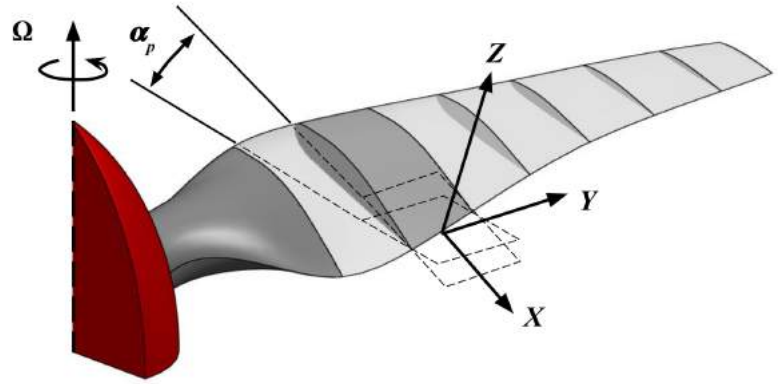


Trailing Edge Noise Formulation

- Starting with Amiet's model for power:

$$S_{pp(U/L)} = \left(\frac{\omega}{a}\right)^2 c^2 dr \left(\frac{1}{32\pi^2}\right) \frac{N_B}{2\pi} \int_0^{2\pi} D_\phi |L|^2 l_r \Phi_{pp} d\phi$$

  - U, L – upper and lower surfaces of an airfoil
  - D – spectrum directivity
  - ϵ – doppler shifted frequency
  - c – chord length of the blade section
  - L – loading term
  - Φ_{PP} – Lee's wall pressure spectrum model using 2D panel code

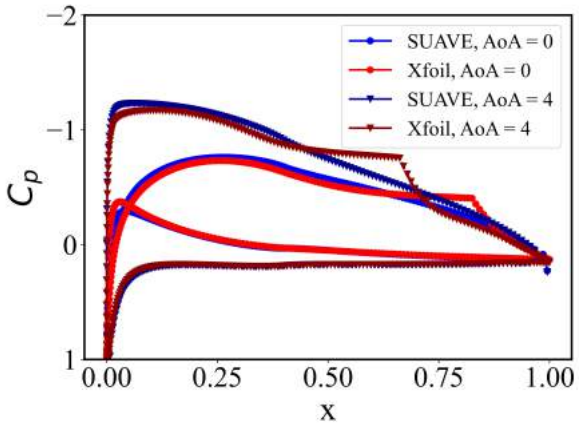


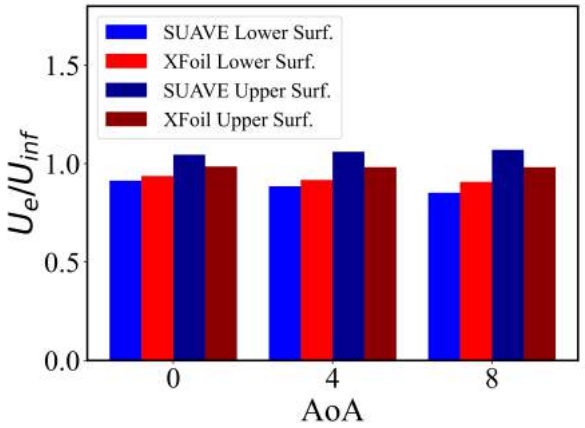
- The far-field SPL for one side of the i^{th} section on the n^{th} rotor blade is calculated from the acoustic power spectral density S_{pp} as

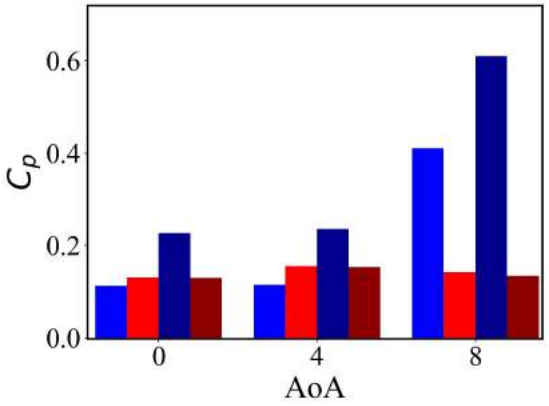
$$\mathrm{SPL}_{\mathrm{bb}_{i(U,L)}} = 10 \log_{10} \left(\frac{2\pi S_{pp(U,L)}}{P_0^2}\right)$$

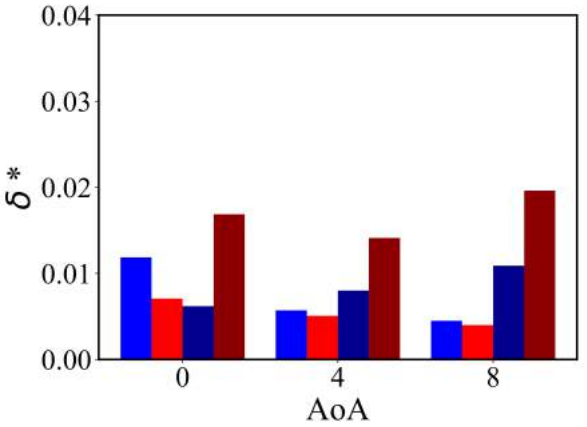
Computation of Blade Section Boundary Layer Properties

- Wall Pressure Spectrum Model requires boundary layer properties of the rotor blade section boundary layer: $\theta, \delta, \delta^*, {}^{U_e}/_{U_\infty}, c_f$ and ${}^{dP}/_{dx}$
- Developed a vectorized panel method code capable of computing properties across an arbitrary lifting surface.
  - Uses Thwaites (laminar) and Head (turbulent) method with Mitchel Criteria (transition)







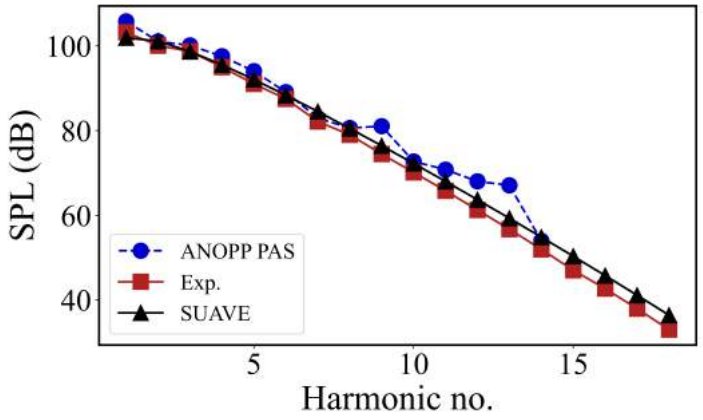


Validation: Harmonic Noise

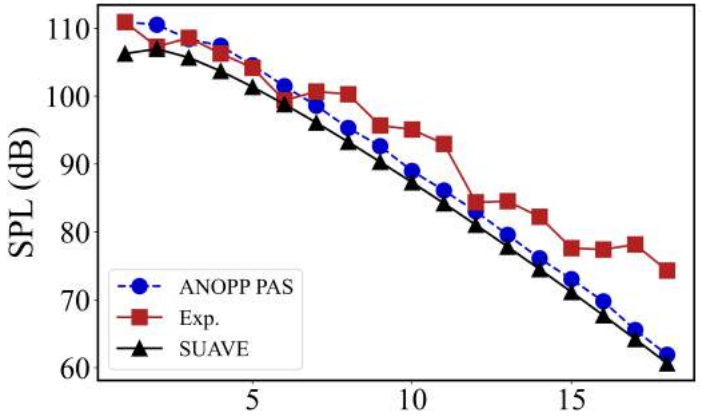
- Test 1 (Strength)
  - Source: Weir, D., and J. Powers. "Comparisons of predicted propeller noise with wind tunnel and flyover data." *25th AIAA Aerospace Sciences Meeting*. 1987.
  - Rotor: 2-bladed, 2.03 m dia. Hartzell Propeller
  - Test Conditions: 3 Cases (C_p = 0.027 ,0.047 and 0.042) at $\theta_{mic} = 60° \ \& \ 90°$
- Test 2 (Directivity)
  - Source: Hubbard, Harvey H. *Sound measurements for five shrouded propellers at static conditions*. No. 2024. National Advisory Committee for Aeronautics, 1950.
  - Rotor: 2-bladed, 1.21 m dia. Hubbard Propeller
  - Test Conditions: Microphones measuring the directivity of the first two harmonics ($0° \leq \theta_{mic} \leq 180°$)

Validation: Harmonic Noise – B.P.F Strength

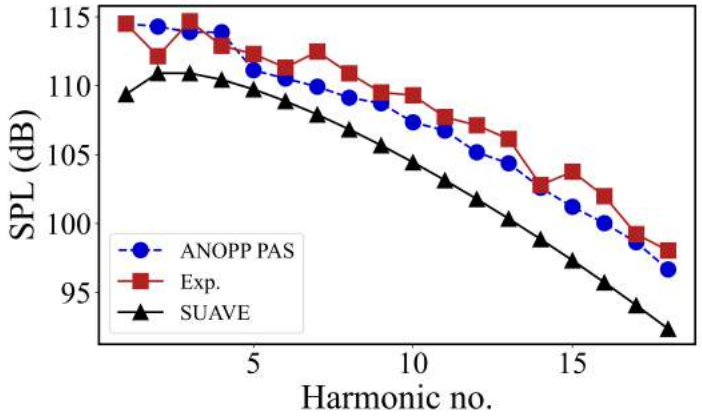
$C_T = 0.027,\ \theta_{mic} = 60\ °$



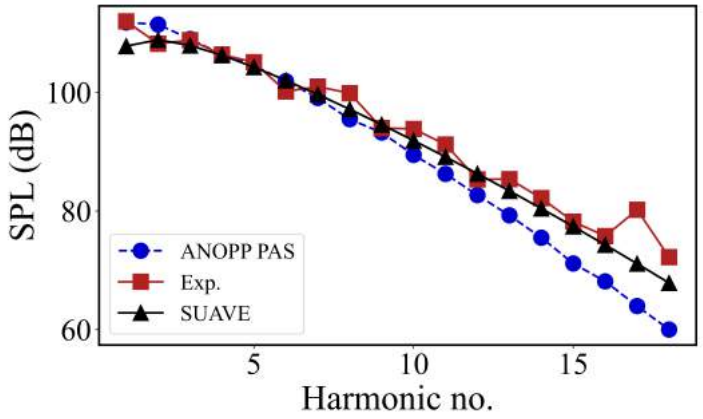
$C_T = 0.047, \theta_{mic} = 60\ °$



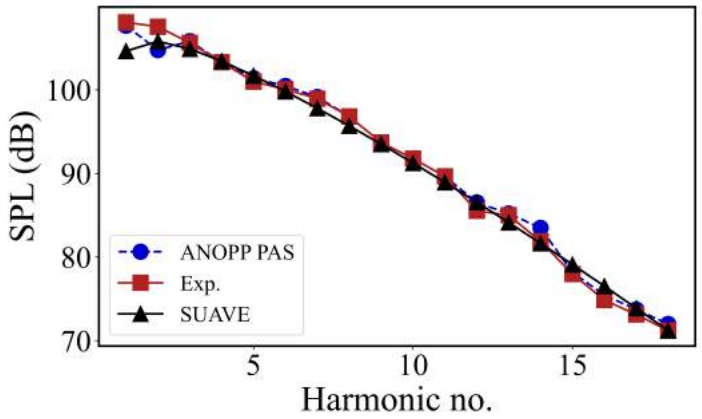
$C_T = 0.042, \theta_{mic} = 60\ °$



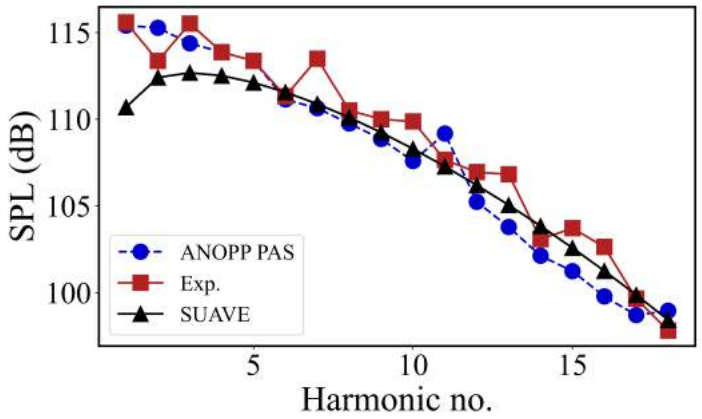
$C_T = 0.027,\ \theta_{mic} = 90\ °$



$C_T = 0.047,\ \theta_{mic} = 90\ °$

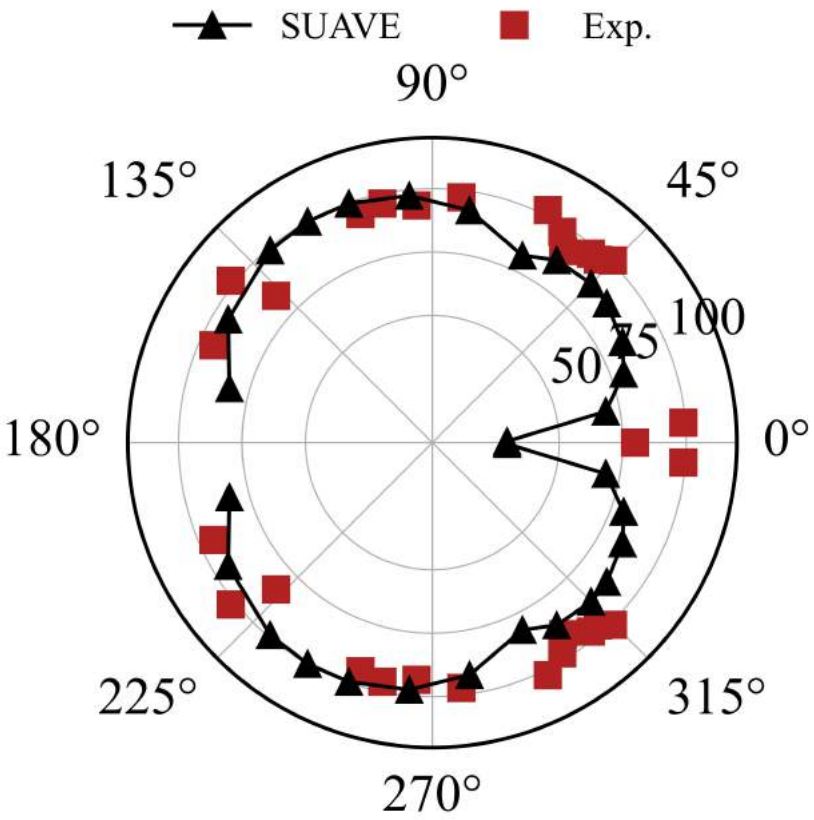


$C_T = 0.042,\ \theta_{mic} = 90\ °$

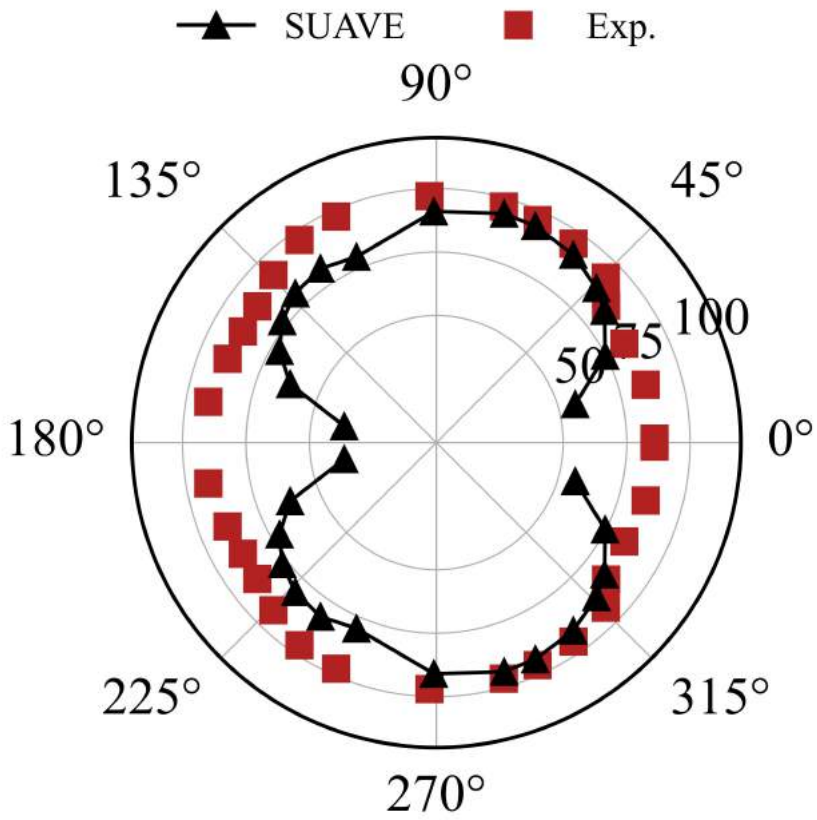


Validation: Harmonic Noise – Directivity

1st Harmonic

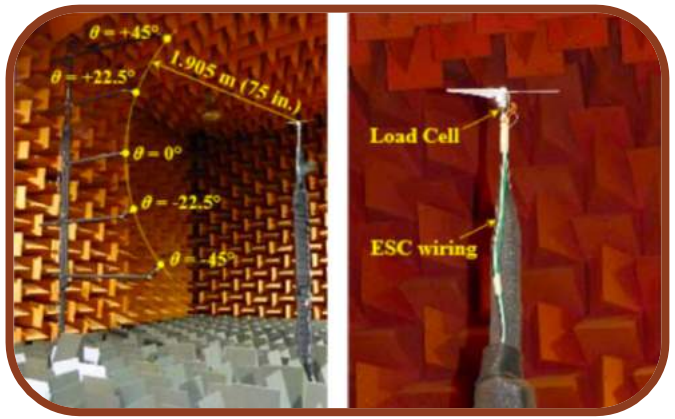


2nd Harmonic

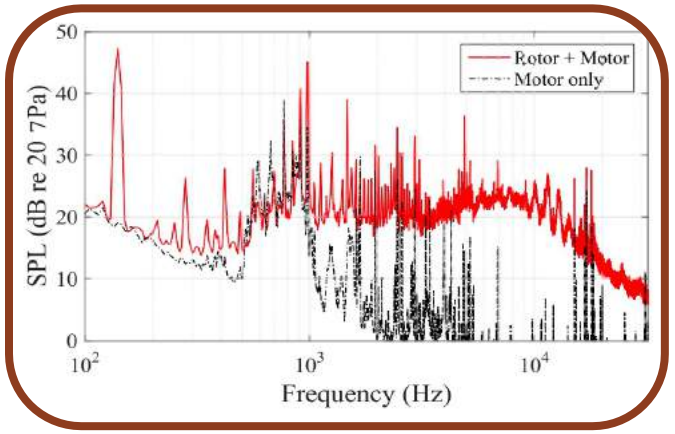


Validation: Broadband Noise

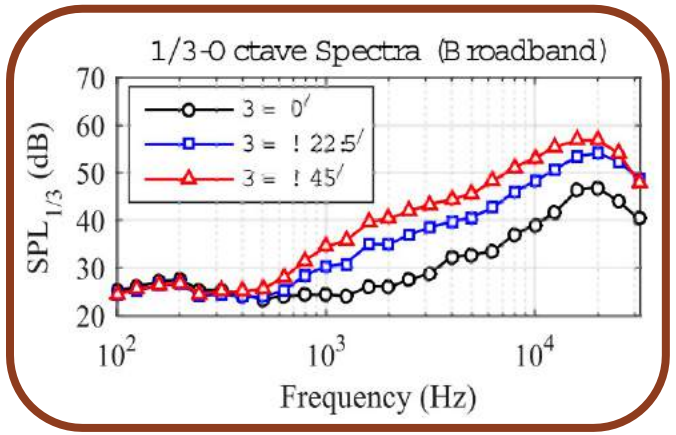
- Source: Zawodny, Nikolas S., D. Douglas Boyd Jr, and Casey L. Burley. "Acoustic characterization and prediction of representative, small-scale rotary-wing unmanned aircraft system components." *American Helicopter Society (AHS) Annual Forum*. No. NF1676L-22587. 2016.
  - Rotor: 2-bladed APC 11x4.7SF rotor, 0.28 m dia.
  - Test Conditions: 4200 RPM at $\theta_{mic} = 22.5° \; and \; 45°$



Experimental apparatus within SALT Facility



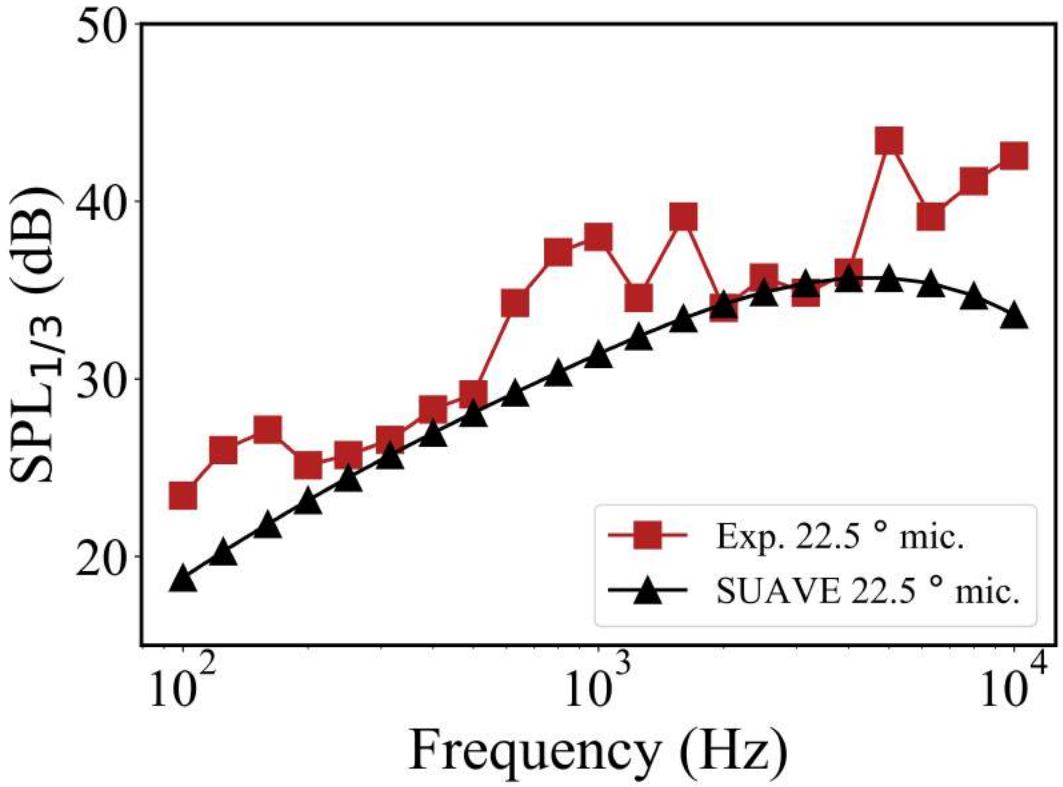
Acoustic narrowband spectra comparison



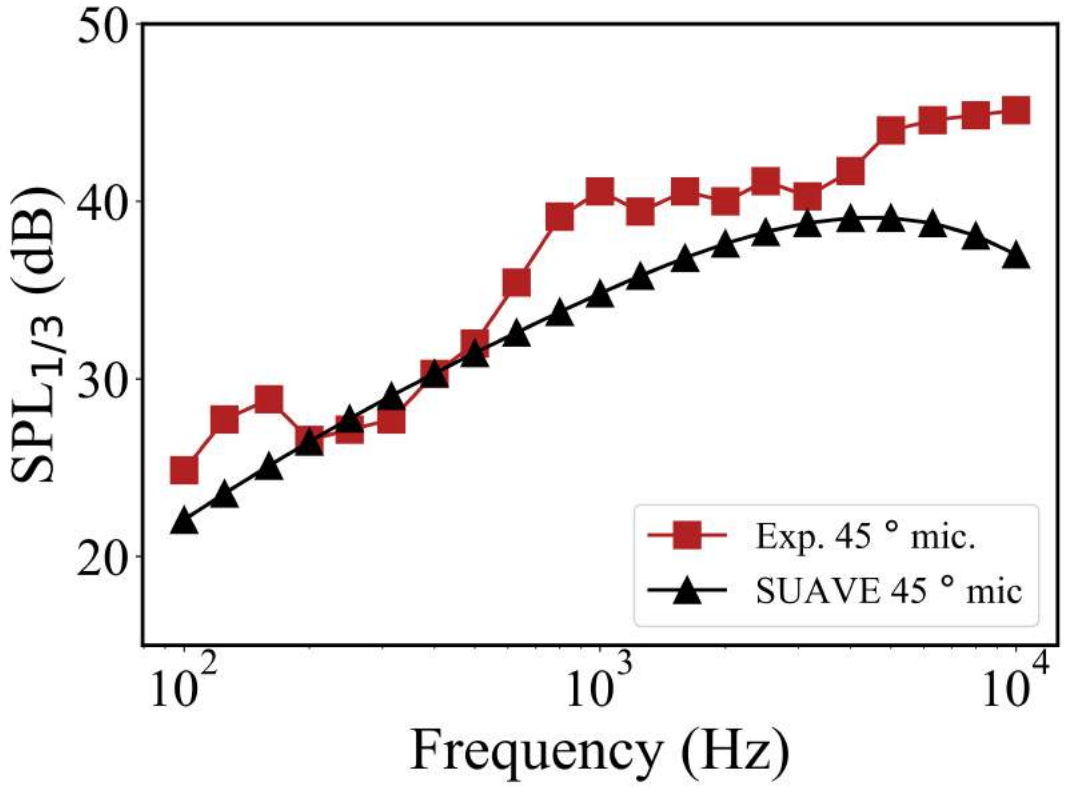
1/3-Octave spectra

Validation: Broadband Noise

$RPM = 4200, \theta_{mic} = 22.5\,°$



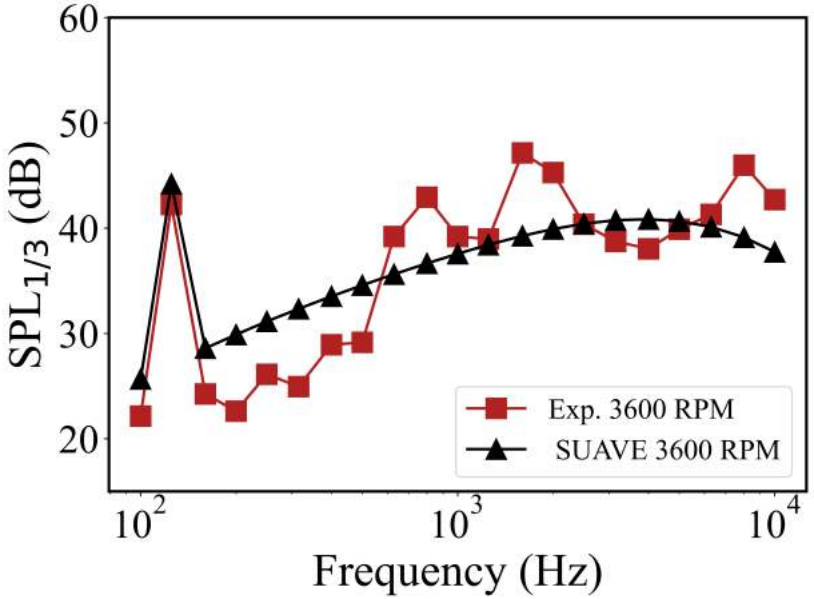
$RPM = 4200, \theta_{mic} = 45°$



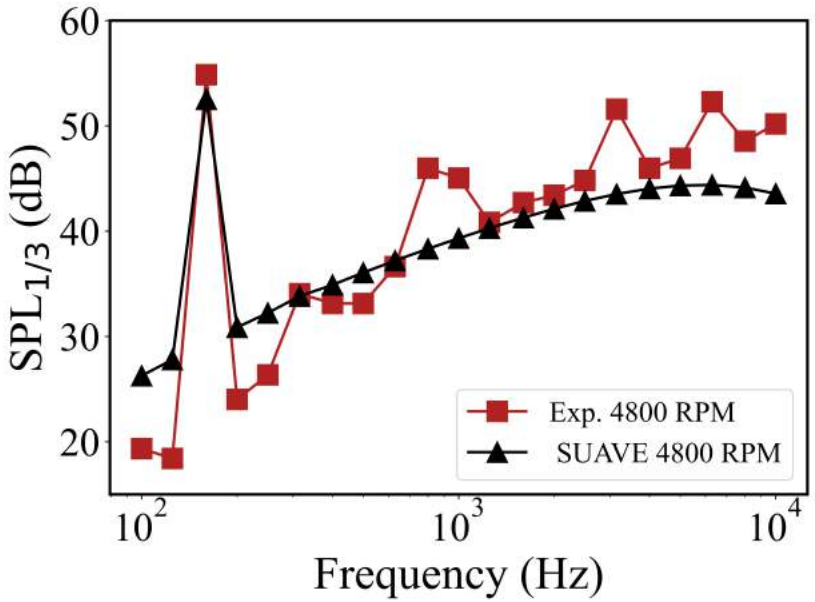
Validation: 1/3 Octave Band Acoustic Spectrum

- Source: Zawodny, Nikolas S., D. Douglas Boyd Jr, and Casey L. Burley. "Acoustic characterization and prediction of representative, small-scale rotary-wing unmanned aircraft system components." *American Helicopter Society (AHS) Annual Forum*. No. NF1676L-22587. 2016.
  - Rotor: 2-bladed APC 11x4.7SF rotor, 0.24 m dia.

$RPM = 3600, \theta_{mic} = 45\,°$

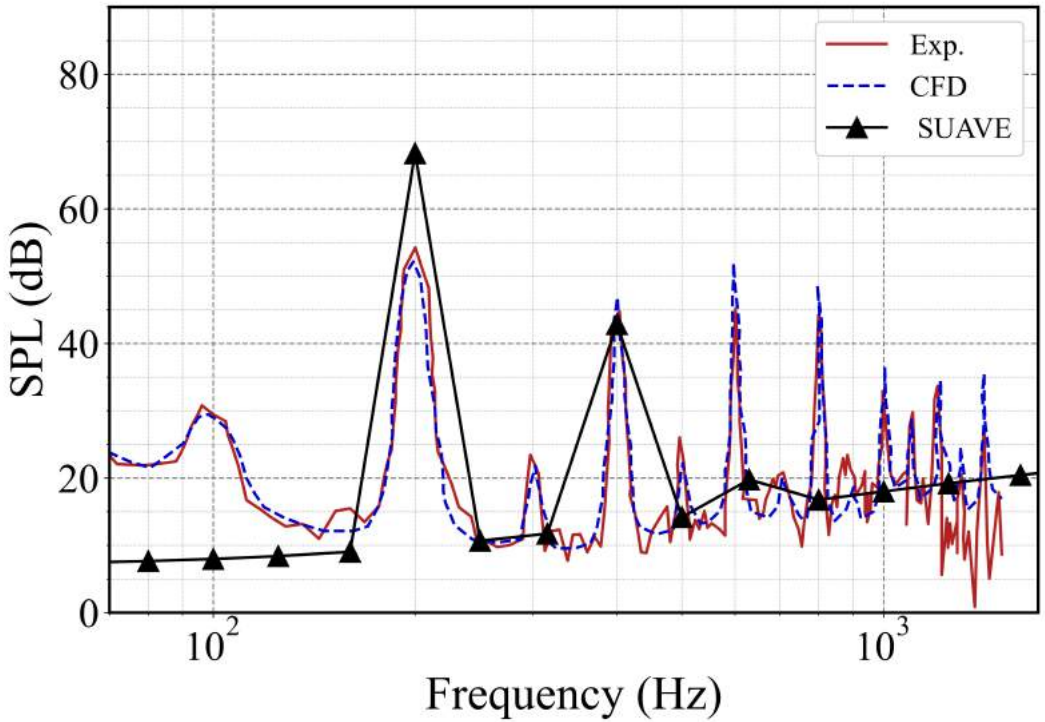


$RPM = 4800, \theta_{mic} = 45°$



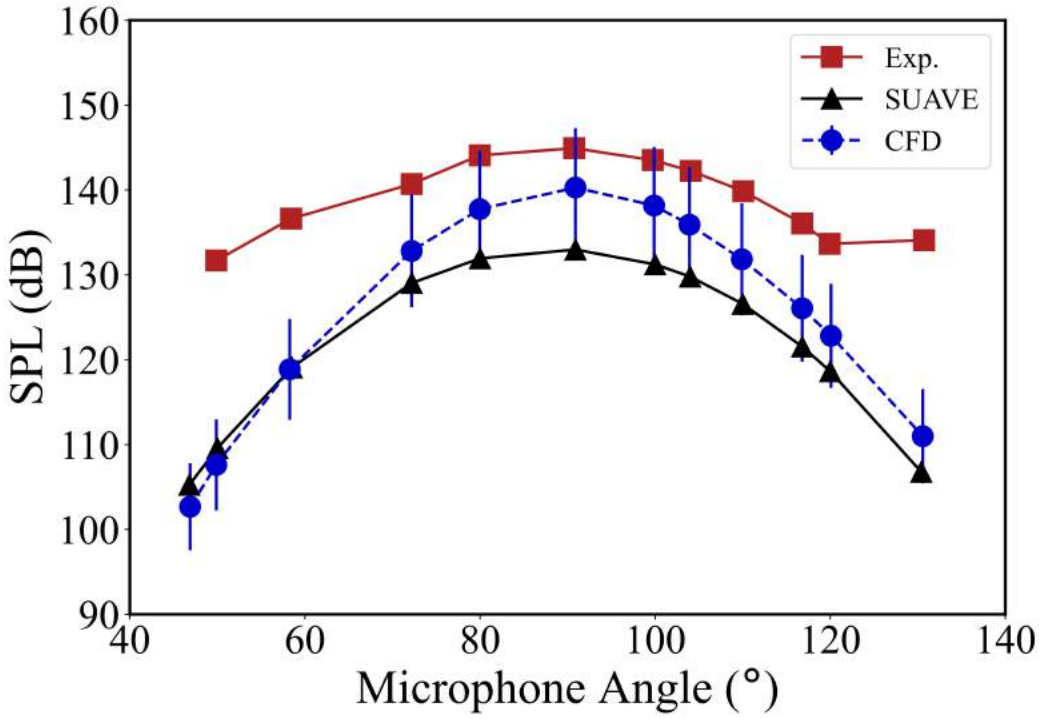
Validation: Comparisons to High-Fidelity CFD Models

Simulation Time of DES with RANS turbulence model: 2250 CPU-hours (78 million cell model), Mankbadi, 2021.



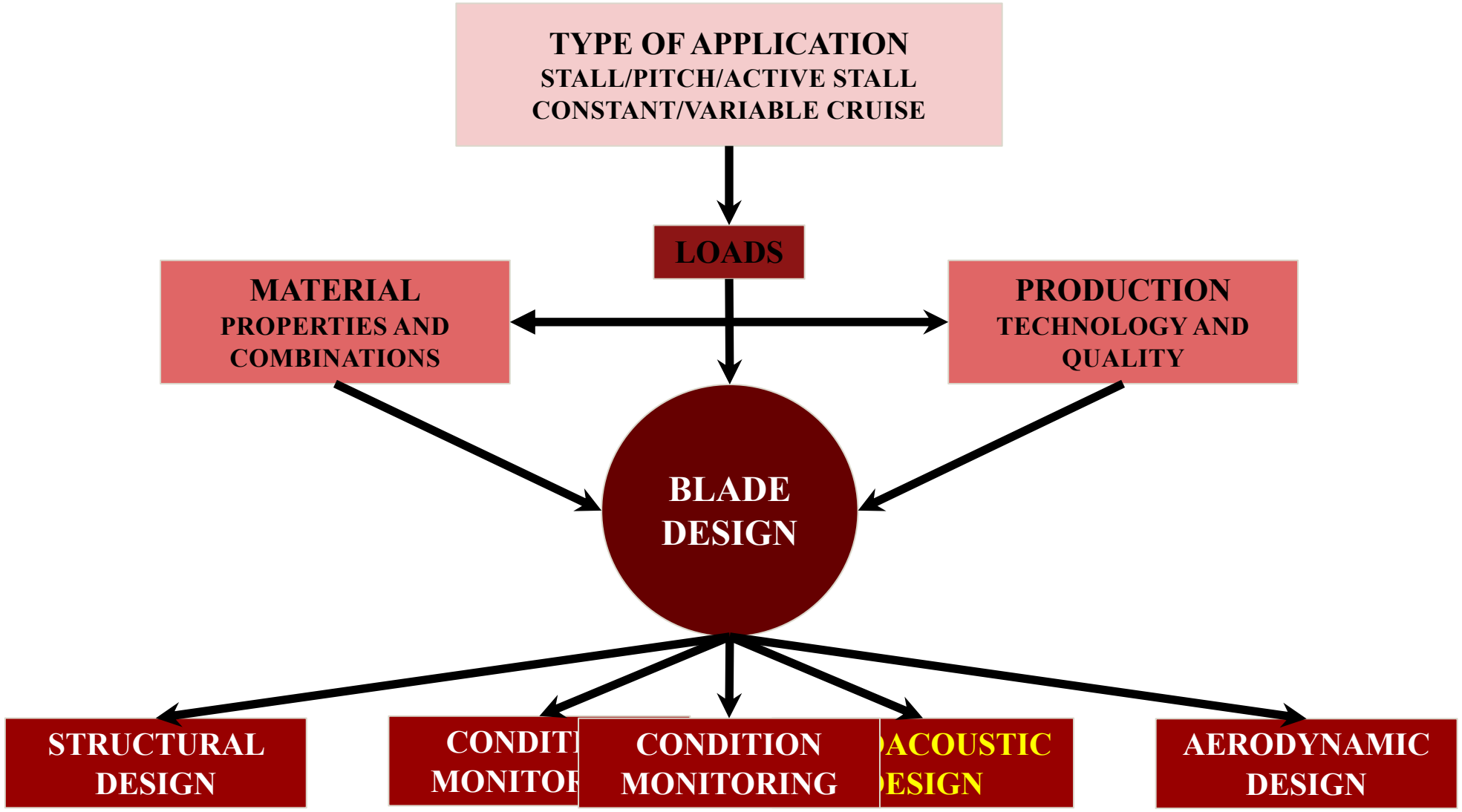
3.83 sec

Simulation Time of hybrid LES-URANS: 650 CPU hours (360 CPU cores in parallel), Tan 2014



6.22 sec

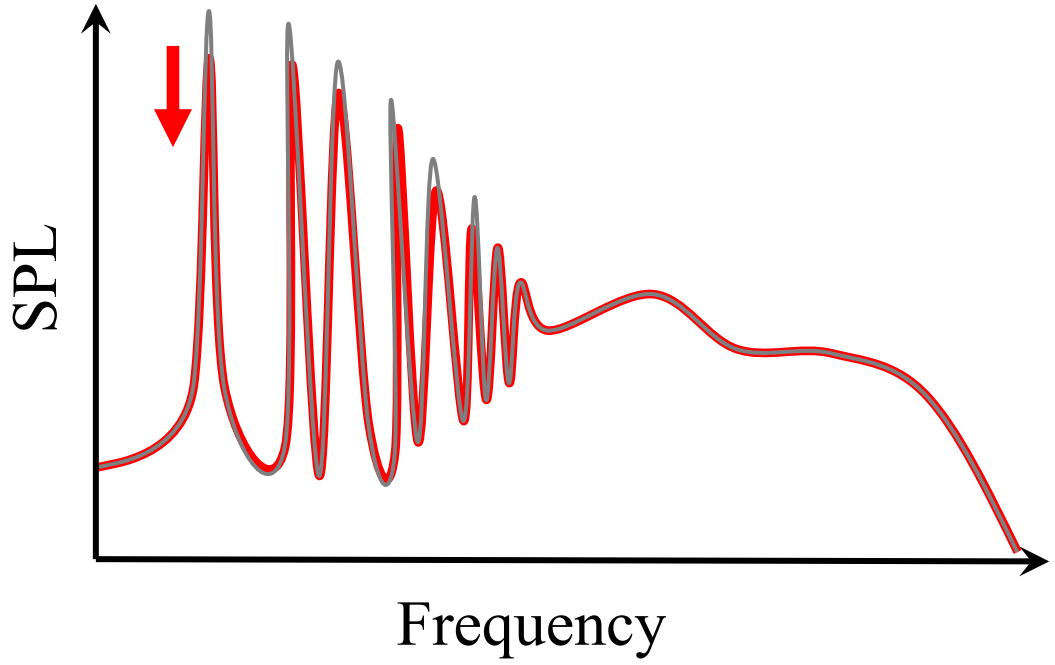
Rotor Design Considerations

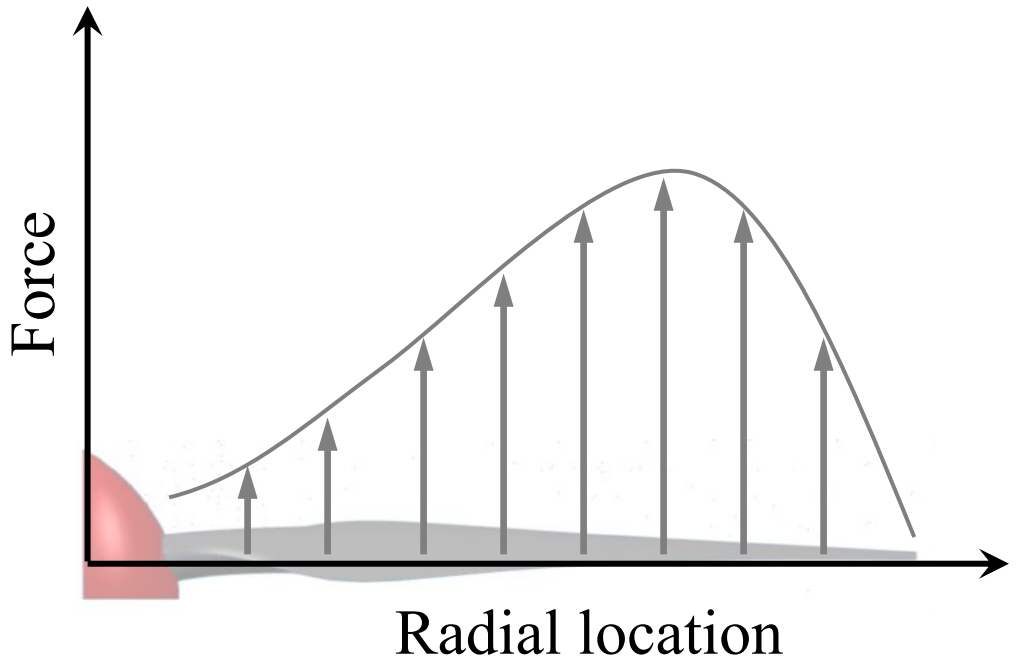


Adapted from Scherer (1999), Renewable Energy

Parametric and Load Sensitivity on Acoustic Spectrum and Aerodynamic Efficiency

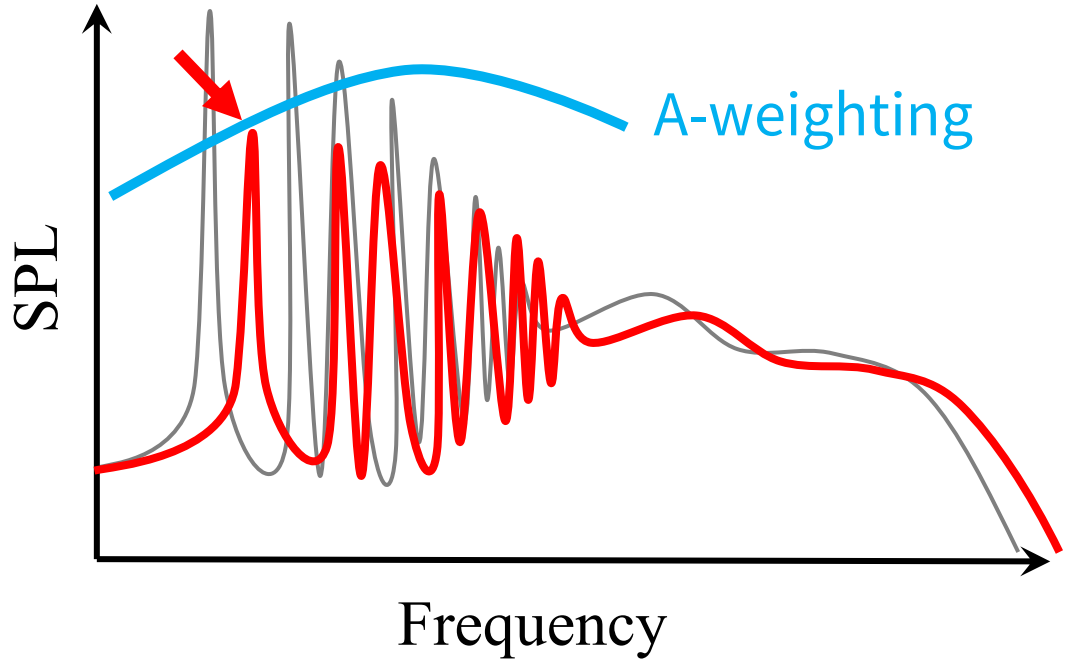
Variable	Acoustics Impact	Aerodynamic Impact
Blade Solidity, σ	Low σ reduces thickness noise as volume displaced by each blade decreases.	Decreasing σ improves efficiency. If σ is too low, however, high AoA is needed to achieve required lift.

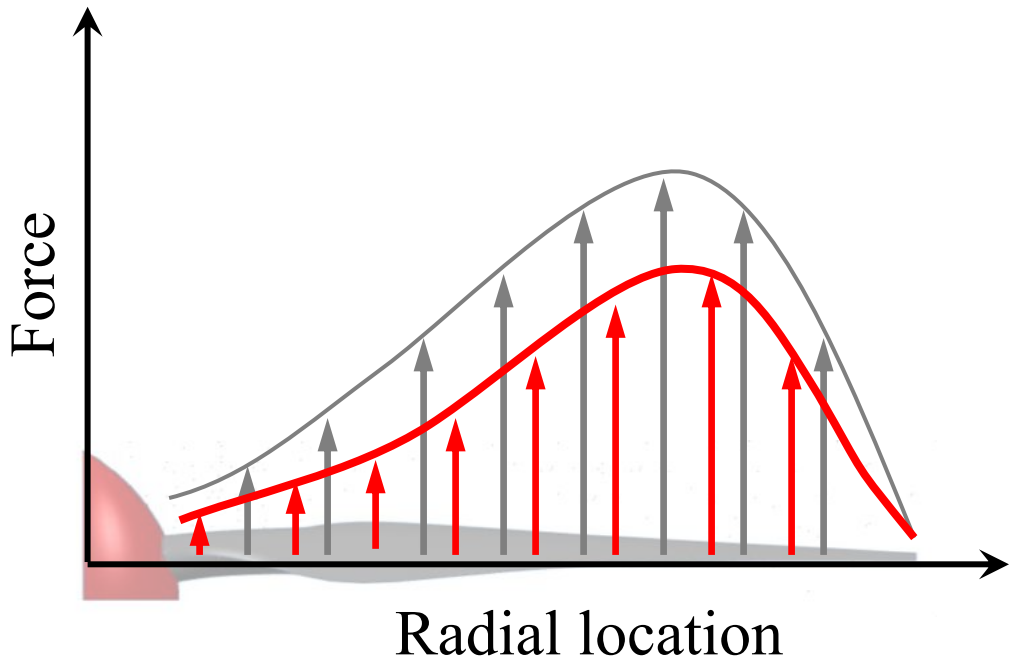




Parametric and Load Sensitivity on Acoustic Spectrum and Aerodynamic Efficiency

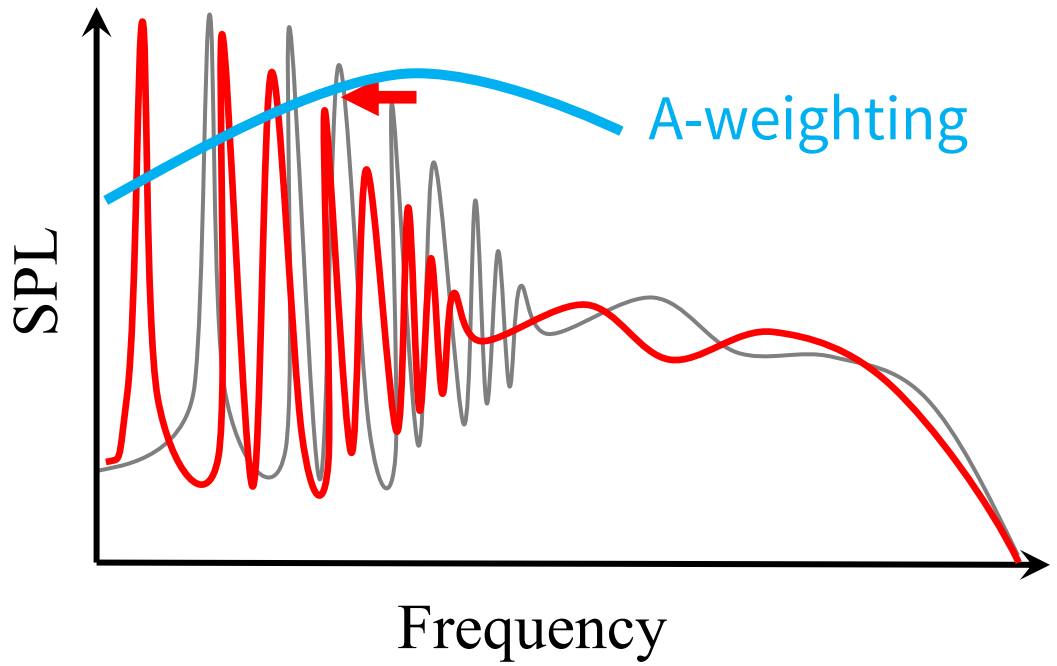
Variable	Acoustics Impact	Aerodynamic Impact
Number of Blades, B	Increasing B increases B.P.F which diminishes the effect of A-weighting scaling	Increasing B reduces the efficiency of the rotor due to wake interference and aerodynamic drag.

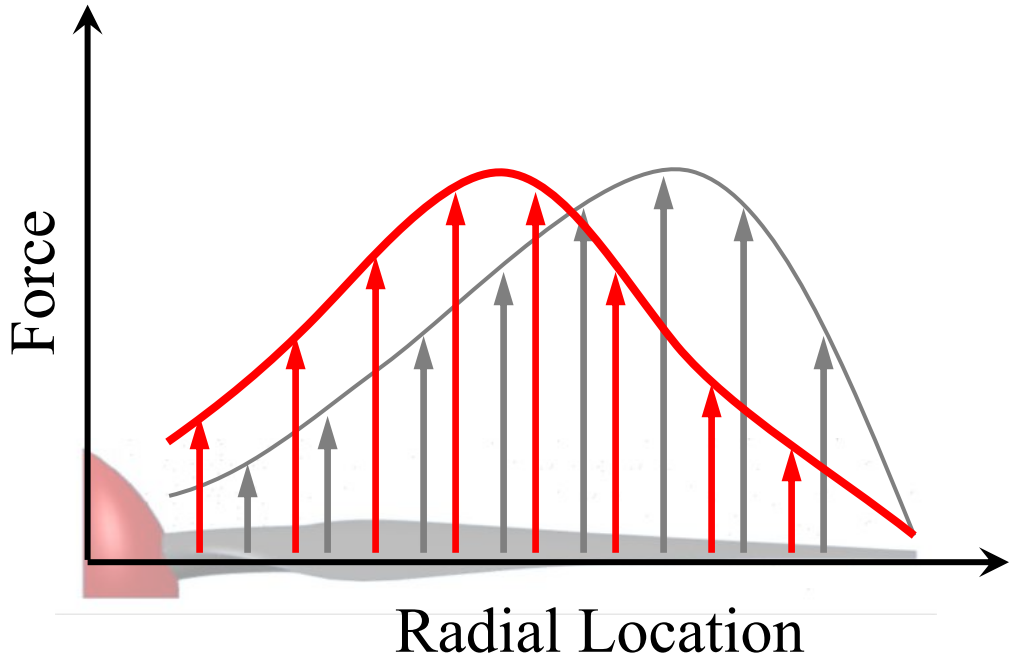




Parametric and Load Sensitivity on Acoustic Spectrum and Aerodynamic Efficiency

Variable	Acoustics Impact	Aerodynamic Impact
Blade Twist, $\beta(r)$	Retwisting the blade to move $T(r)$ inboard leads to a redistribution of harmonic strength	Shifting load inboard reduces efficiency





Rotor Blade Design Optimization: Lift-Rotor Case

$$\min \quad f(X) \text{ where, } f = \left(\left|\frac{(FM - FM^*)}{FM^*}\right|\right)\alpha + \left(\left|\frac{(\overline{SPL} - SPL^*)}{SPL^*}\right|\right)(1-\alpha)$$

aero. acous.

$$\text{s.t.} \quad T = T_{design}$$

$$C_{l_{max}} \leq 0.8$$

$$0.3 \leq \lambda \leq 0.7$$

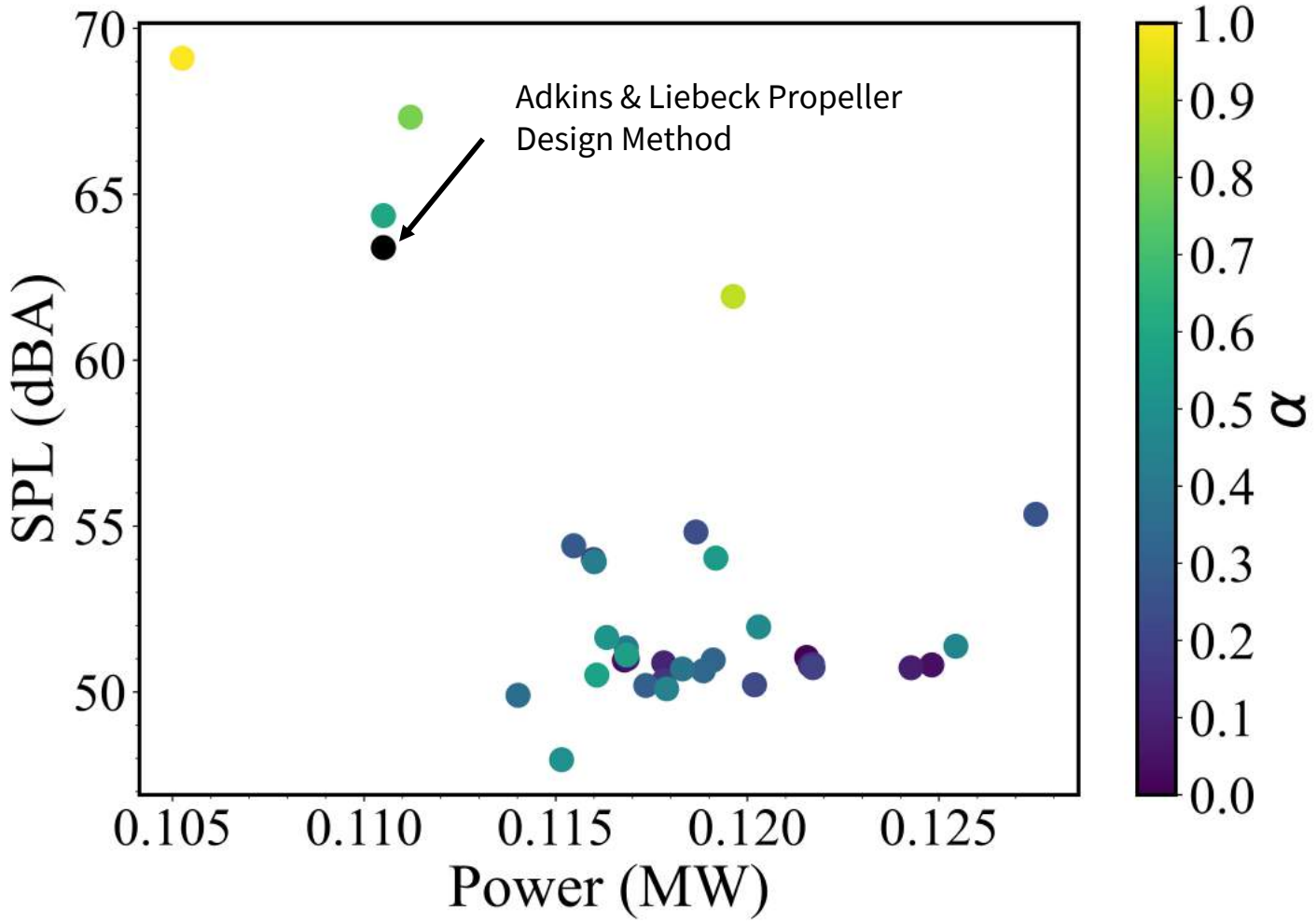
$$\frac{c_p}{c_q} \geq 0.5$$

$$\frac{\beta_p}{\beta_q} \geq 0.5$$



- Aircraft MTOW = 27000 N
- Number of rotors (r) = 12
- Design Load = MTOW/(n-2)
- Number of blades (b) = 3
- Max sectional C_l = 0.8
- Inflow ratio, λ = 0.05
- Design Tip Speed = 0.65
- Blade tip radius = 1.25 m
- Section airfoil = NACA 4412
- Aeroacoustic weight, $\alpha \in [0,1]$

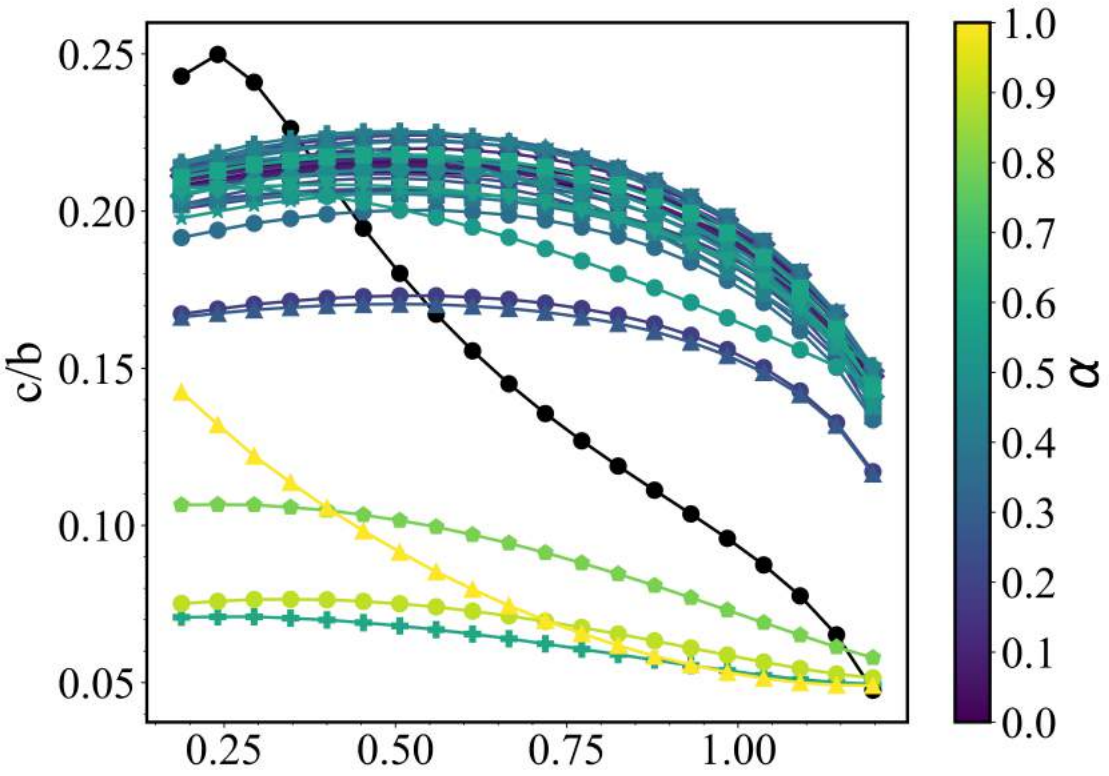
Rotor Blade Design Optimization: Results



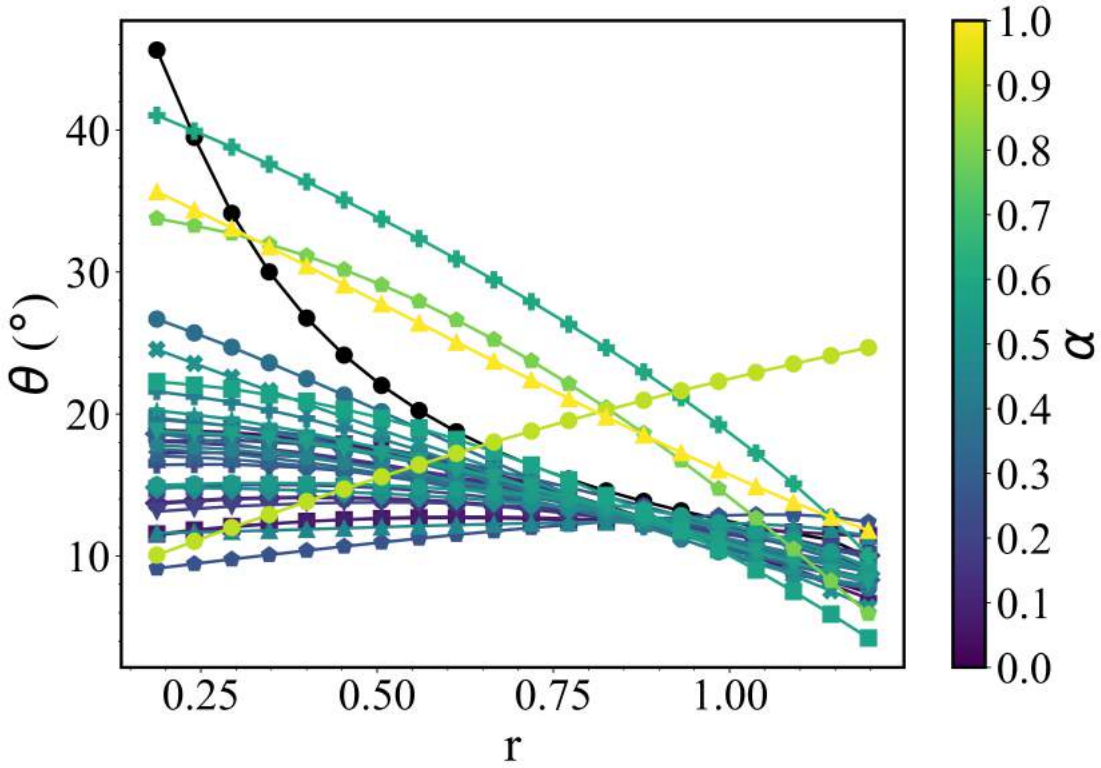
- High α generates aerodynamically efficient blade designs
- Low α prioritizes rotor noise reduction

Rotor Blade Design Optimization: Results

Blade Chord Distribution



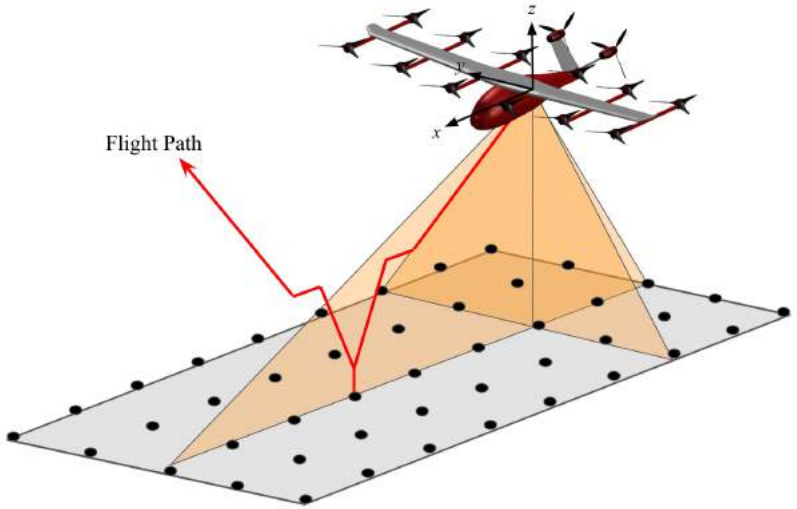
Blade Twist Distribution

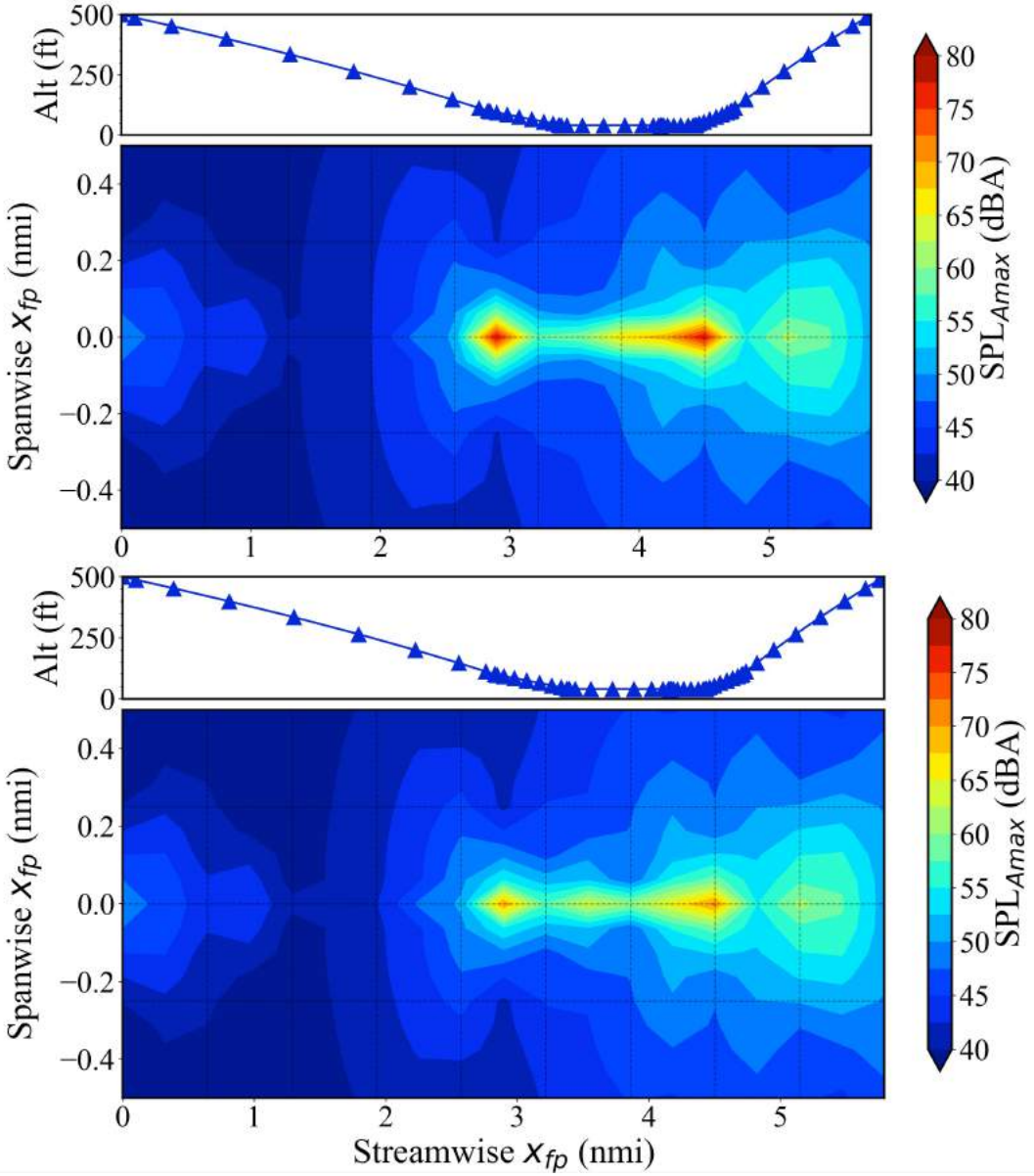


Rotor Blade Design Optimization: Results



Stopped-Rotor Approach & Departure Noise



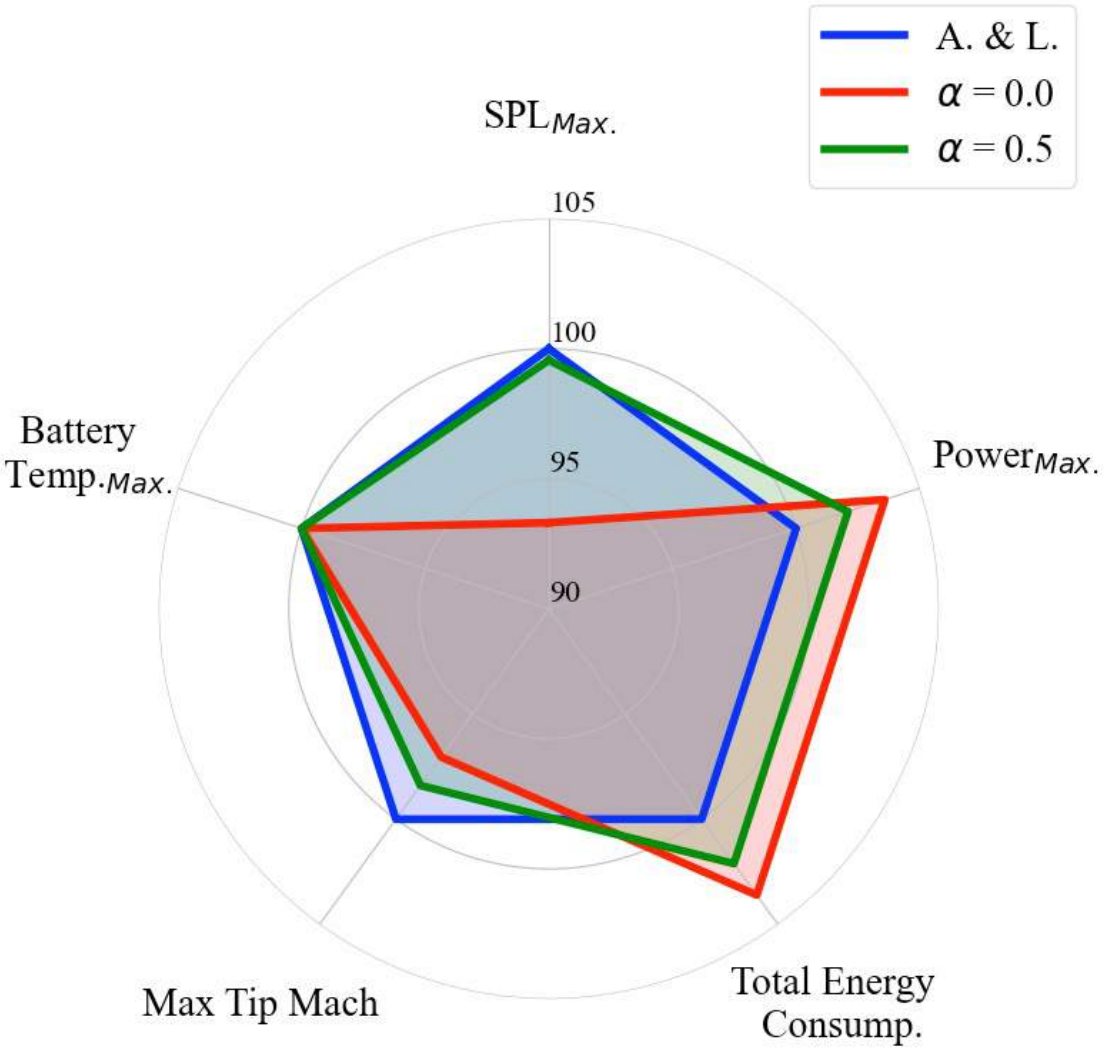


Baseline

$\alpha = 0.5$

Comparison of Performance Metrics

- Examining the vertical climb segment only, we observe:
  - 2.5 % reduction in blade tip Mach No.
  - 6.4 % reduction in vehicle noise
  - 3% increase in maximum power
  - 3.1% increase in total energy consumed



Future Work



Flight trajectory optimization encompassing desired noise emissions and battery cell degradation (temporal) targets



Urban canyon and digital elevation model noise prediction



Exploring nuances of multi-disciplinary coupling and broader economic impact

Concluding Remarks

- Integration of medium-fidelity techniques can inform critical design choices at an earlier stage of the design process.
- Implemented computational approaches can be applied to problems beyond the scope of regional and urban air mobility.
  - Propfan aircraft (acoustics)
  - UAS, PEVs (batteries)





Thank You

Questions ?

MCLARKE2@STANFORD.EDU

aerospacedesignlab

References

1. Hamilton, Booz Allen. "Final Report Urban Air Mobility (UAM) Market Study." *National Aeronautics and Space Administration: McLean, WA, USA* (2018).
2. National Academies of Sciences, Engineering, and Medicine. *Advancing aerial mobility: A national blueprint*. National Academies Press, 2020.
3. Leishman, Gordon J. Principles of helicopter aerodynamics with CD extra. Cambridge university press, 2006.
4. Hanson, D. B. "Sound from a propeller at angle of attack: a new theoretical viewpoint." Proceedings of the Royal Society of London. Series A: Mathematical and Physical Sciences 449.1936 (1995): 315-328.
5. Brooks, Thomas, and Casey Burley. "Rotor broadband noise prediction with comparison to model data." 7th AIAA/CEAS Aeroacoustics Conference and Exhibit. 2001.
6. Brooks, Thomas, and Casey Burley. "Rotor broadband noise prediction with comparison to model data." 7th AIAA/CEAS Aeroacoustics Conference and Exhibit. 2001.
7. Saetti, Umberto. "Rotorcraft simulations with coupled flight dynamics, free wake, and acoustics." (2016).
8. “Carbon Pollution from Transportation,” , Jun 2019. URL https://www.epa.gov/transportation-air-pollution- and-climate-change/carbon-pollution-transportation.
9. NASA, “Why Build an Electric Airplane?” , 2019. URLhttps://www.nasa.gov/specials/X57/electric-airplane.html
10. Chin, J. C., Schnulo, S. L., Miller, T. B., Prokopius, K., and Gray, J., “Battery Performance Modeling on Maxwell X-57,” AIAA Scitech, San Diego, CA, 2019.
11. Hannan, M. A., Hoque, M. M., Hussain, A., Yusof, Y., and Ker, P. J., “State-of-the-Art and Energy Management System of Lithium-Ion Batteries in Electric Vehicle Applications: Issues and Recommendations,” IEEE Access, Vol. 6, 2018, pp. 19362–19378. doi:10.1109/ACCESS.2018.2817655.
12. Bernardi, D., Pawlikowski, E., and Newman, J., “General Energy Balance for Battery Systems.” Electrochemical Society Extended Abstracts, Vol. 84-2, 1984, pp. 164–165.
13. Schmalstieg, J., Käbitz, S., Ecker, M., and Sauer, D. U., “A holistic aging model for Li(NiMnCo)O2 based 18650 lithium-ion batteries,” Journal of Power Sources, Vol. 257, 2014, pp. 325–334. doi:10.1016/j.jpowsour.2014.02.012.
14. Traub, Lance W., et al. "Effect of taper ratio at low reynolds number." *Journal of Aircraft* 52.3 (2015): 734-747.
15. Scherer, Roger. "Blade design aspects." *Renewable energy* 16.1-4 (1999): 1272-1277.